

---

# CRPS-LAM: Regional ensemble weather forecasting from matching marginals

---

**Erik Larsson**

Linköping University, Sweden  
erik.larsson@liu.se

**Joel Oskarsson**

Linköping University, Sweden  
joel.oskarsson@outlook.com

**Tomas Landelius**

SMHI, Sweden  
tomas.landelius@smhi.se

**Fredrik Lindsten**

Linköping University, Sweden  
fredrik.lindsten@liu.se

## Abstract

Machine learning for weather prediction increasingly relies on ensemble methods to provide probabilistic forecasts. Diffusion-based models have shown strong performance in Limited-Area Modeling (LAM) but remain computationally expensive at sampling time. Building on the success of global weather forecasting models trained based on Continuous Ranked Probability Score (CRPS), we introduce CRPS-LAM, a probabilistic LAM forecasting model trained with a CRPS-based objective. By sampling and injecting a single latent noise vector into the model, CRPS-LAM generates ensemble members in a single forward pass, achieving sampling speeds up to  $39\times$  faster than a diffusion-based model. We evaluate the model on the MEPS regional dataset, where CRPS-LAM matches the low errors of diffusion models.

## 1 Introduction

Machine learning methods for simulating atmospheric dynamics are revolutionizing modern weather forecasting [Bi et al., 2023, Lam et al., 2023, Lang et al., 2024a, Price et al., 2025, Lang et al., 2024b, Bonev et al., 2025]. Offering fast and accurate forecasts, these Machine learning Weather Prediction (MLWP) methods have great potential for predicting and understanding both everyday weather conditions and extreme events. While initial MLWP methods used deterministic models to produce single forecasts [Bi et al., 2023, Lang et al., 2024a], the field is increasingly moving towards more useful ensemble forecasting models [Price et al., 2025, Lang et al., 2024b, Bonev et al., 2025, Alet et al., 2025]. These methods use conditional generative models to sample forecasts from the distribution of possible future atmospheric states. Such sampled ensemble members can then be used to estimate probabilities of specific atmospheric conditions, or studied by meteorologists in order to understand possible future scenarios. These developments towards MLWP ensemble forecasting are happening both for the global domain, and for the regional setting considered in this work. Regional MLWP allows for building high-resolution models without excessive computational and memory costs, while enabling training on high-quality region-specific datasets.

Initial attempts at MLWP ensemble forecasting for regional domains have either failed to reproduce all high-frequency details [Oskarsson et al., 2024] or used computationally expensive diffusion models [Pathak et al., 2024, Larsson et al., 2025]. Building on methodology proven successful for global forecasting [Alet et al., 2025], we show that such a regional ensemble forecasting model can be trained by matching only marginal distributions through a loss function based on the Continuous Ranked Probability Score (CRPS). We propose a regional weather forecasting model where a single

latent noise vector introduces stochasticity in the model, allowing for sampling realistic ensemble members in only a single forward pass through the network.

**Problem definition.** In this paper, we address the problem of probabilistic MLWP in the context of Limited-Area Modeling (LAM), following the formulation of Larsson et al. [2025]. In LAM forecasting, the data is a gridded representation of a region of interest with positions  $G$ . The atmospheric state at lead time  $t$  is denoted by  $X^t \in \mathbb{R}^{|G| \times d_x}$ , where  $d_x$  denotes the number of variables per grid point. The model also uses time-dependent forcing inputs  $F^t$  (e.g., time of day) and static spatial fields  $S$  (e.g., orography and land–sea mask). To separate the area of prediction from the boundary, we define an interior region input  $I^t = \{X_I^{t-1:t}, F_I^{t-1:t+1}, S_I\}$  and a boundary region input  $B^t = \{X_B^{t-1:t+1}, F_B^{t-1:t+1}, S_B\}$  (see Fig. 1). To generate ensemble forecasts for the interior region we want to sample from the conditional distribution  $p(X_I^{t+1} | I^t, B^t)$ .

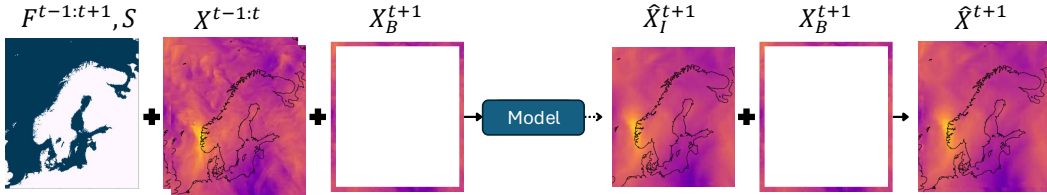


Figure 1: An overview of the forecasting process showing the inputs and outputs of the model (adapted from [Larsson et al., 2025]).

**Our main contributions are:** 1) We introduce a CRPS-based probabilistic model for limited-area weather forecasting, producing forecasts with a fraction of the computational cost of state-of-the-art diffusion models. 2) Through experiments on the MEPS LAM dataset, we demonstrate that our model produces competitive ensemble forecasts that exhibit both fine-scale detail and physically consistent spatial structures.

**Related Work.** Recently, CRPS-based training objectives have been successfully applied to global MLWP models [Pacchiardi et al., 2024, Lang et al., 2024b, 2025, Bonev et al., 2025, Alet et al., 2025, Oskarsson et al., 2024]. These approaches differ primarily in how the CRPS is estimated and how stochasticity is introduced into the model. However, all these methods can produce skillful ensemble forecasts with a single forward pass through the network. A particularly convenient formulation is that of Alet et al. [2025], which employs a similar conditioning mechanism commonly used in diffusion models, thereby enabling a simple transformation from a diffusion-based model to a CRPS-based one.

Previous approaches to probabilistic LAM have primarily relied on diffusion-based methods [Pathak et al., 2024, Larsson et al., 2025, Abdi et al., 2025]. Diffusion models have demonstrated strong forecasting performance, but at substantial computational cost during sampling of ensemble members. The Graph-EFM latent variable model [Oskarsson et al., 2023] is capable of probabilistic LAM forecasting in a single forward pass, similar to our method. Although it also incorporates a CRPS-based regularization term in its training objective, the Graph-EFM training mainly relies on a more involved variational framework.

## 2 Method

Scoring rules provide a principled way to evaluate the quality of probabilistic forecasts. Given a predicted distribution  $p$  and an observed value  $x \sim q$ , a scoring rule  $s(p, x)$  quantifies how well  $p$  agrees with the observation [Gneiting and Raftery, 2007]. We define  $s(p, q) = \mathbb{E}_q[s(p, x)]$  and say that  $s$  is a *proper scoring rule* if it satisfies  $s(q, q) \leq s(p, q)$  for all  $p$  and  $q$ . The scoring rule is *strictly proper* when equality holds only for  $p = q$ , ensuring that the lowest score is only achieved by the true data distribution. In other words, a strictly proper scoring rule prefers forecasts whose ensemble members are sampled from the same distribution as the observed data. Naturally, minimizing such scoring rules is of interest for training probabilistic forecasting models.

One such strictly proper scoring rule is the Continuous Ranked Probability Score [Gneiting and Raftery, 2007], defined as the squared difference between the Cumulative Distribution Function

(CDF)  $F$  of the forecast distribution  $p$ , and the empirical CDF of the observation. For a univariate real-valued distribution, the CRPS is defined as

$$\text{CRPS}(F, x) = \int_{\mathbb{R}} (F(\hat{x}) - \mathbb{1}(\hat{x} \geq x))^2 d\hat{x} = \mathbb{E}_p[|\hat{x} - x|] - \frac{1}{2}\mathbb{E}_{p,p}[|\hat{x} - \hat{x}'|], \quad (1)$$

where the empirical CDF of the observation is given by the step function  $\mathbb{1}(\hat{x} \geq x)$ . The second equality is a reformulation of the CRPS using another independent identical random variable  $\hat{x}' \sim p$ . This formulation can be used as a basis for empirical estimators. For an ensemble forecast  $\{\hat{x}_n\}_{n=1}^N \sim p$  with  $N$  ensemble members and an observation  $x$ , one useful estimator is the *fair* CRPS

$$\text{CRPS}_{\text{fair}}(\{\hat{x}_n\}_{n=1}^N, x) = \frac{1}{N} \sum_{n=1}^N |\hat{x}_n - x| - \frac{1}{2N(N-1)} \sum_{n=1}^N \sum_{n^*=1}^N |\hat{x}_n - \hat{x}_{n^*}|, \quad (2)$$

which provides an unbiased estimate of the CRPS with respect to the number of ensemble members [Ferro, 2014].

We follow the procedure introduced in Alet et al. [2025], where the backbone neural network of a diffusion model is repurposed as a CRPS-based model. Our backbone architecture is almost identical to that of Larsson et al. [2025], with the exception that the noise encoding is implemented as a single linear layer instead of Fourier embeddings. Specifically, a noise vector of 32 dimensions is sampled as  $z \sim \mathcal{N}(0, I)$ , transformed through a linear layer, and injected into the network via conditional normalization layers [Chen et al., 2021, Song et al., 2021, Karras et al., 2022]. Given the interior state  $I^t$  and boundary conditions  $B^t$ , the network then generates probabilistic forecasts of the interior at the next time step  $I^{t+1} \sim p(X_I^{t+1} | I^t, B^t)$ . To extend forecasts to longer horizons, we employ an autoregressive rollout strategy, where predicted states are recursively used as inputs for subsequent steps.

**Training.** Our training objective is the CRPS, and since our forecasts are represented by empirical ensemble distributions we use the unbiased fair CRPS estimator proposed by Ferro [2014]. Our CRPS loss is thereby defined as

$$\mathcal{L}_{g,d} = \frac{1}{N} \sum_{n=1}^N |\hat{X}_{g,d,n} - X_{g,d}| - \frac{1}{2N(N-1)} \sum_{n=1}^N \sum_{n^*=1}^N |\hat{X}_{g,d,n} - \hat{X}_{g,d,n^*}|, \quad (3)$$

for each grid point  $g \in G_I$  and variable  $d \in d_x$ , where  $N$  denotes the number of ensemble members and  $\hat{X}$  the predicted state. We compute the loss averaged over the spatial dimensions and summed across all variables. We train first for single-step prediction and then using autoregressive rollouts up to time step 2, where the loss is averaged across both time steps, following the approach of Oskarsson et al. [2024]. While Eq. (3) can be minimized by only matching marginal distributions for each location and variable, similarly to [Alet et al., 2025] we rely on the fact that all outputs depend on the same noise vector  $z$  to correctly capture the joint forecast distribution. Additionally, our architecture, which utilizes convolutional neural networks, shares weights across spatial locations, thereby promoting spatially coherent forecasts.

### 3 Experiments

The models<sup>1</sup> are evaluated on the MEPS LAM dataset<sup>2</sup>, using Root Mean Squared Error (RMSE), CRPS, Spread-Skill Ratio (SSR), and a spectral analysis of the produced forecasts. We refer to Larsson et al. [2025] for details about the MEPS dataset and metric definitions. We compare the forecasting performance of CRPS-LAM to the Diffusion-LAM [Larsson et al., 2025] diffusion model and the Graph-EFM latent variable model [Oskarsson et al., 2024]. All forecast trajectories are initialized from the ground-truth states and generated autoregressively up to a lead time of 57 h, with 25 ensemble members produced for each model. The model is trained to perform 3 h forecasts (see Fig. 1) and is rolled out autoregressively to produce longer forecasts. CRPS-LAM can generate 57 h forecasts in approximately 0.5 s per ensemble member on a single A100 GPU. Moreover, an

<sup>1</sup>The code and implementation details will be made publicly available upon acceptance of this paper at <https://github.com/ErikLarssonDev/neural-lam/tree/CRPS-LAM>.

<sup>2</sup>The MEPS dataset is openly available at <https://nextcloud.liu.se/s/meps>

arbitrary number of ensemble members can be sampled in parallel through batched inference on one or multiple GPUs. This corresponds to a sampling speed comparable to that of Graph-EFM or a deterministic model (on a per-member basis) and approximately  $39\times$  faster than Diffusion-LAM, depending on the number of solver steps that are used. The results show that CRPS-LAM achieves performance competitive with both Diffusion-LAM and Graph-EFM in terms of the sample quality exemplified in Fig. 2, as well as pixelwise performance metrics in Fig. 3.

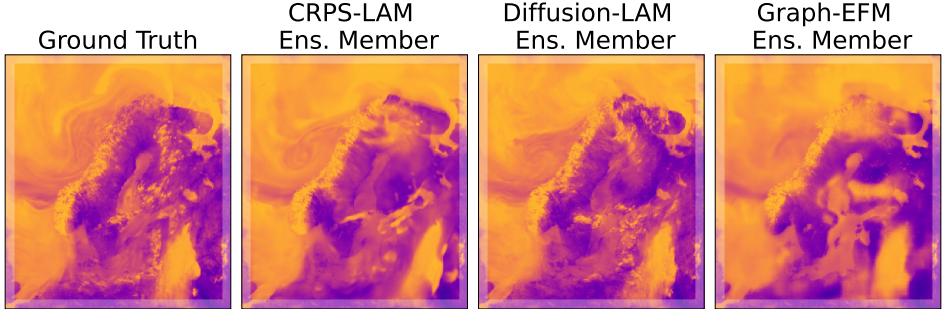


Figure 2: Forecasts at 57 h lead time for  $r_2$ . The faded area constitutes the boundary region.

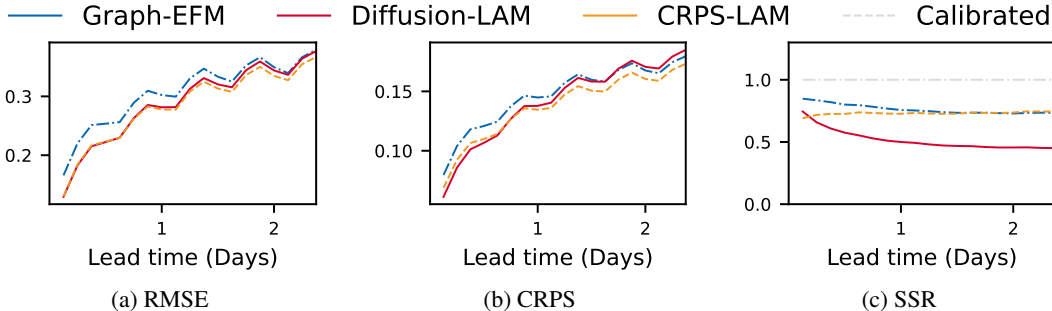


Figure 3: The mean of the normalized RMSE, CRPS, and SSR for all variables.

CRPS-LAM shows low errors, comparable with Diffusion-LAM, while retaining the fast inference speed of Graph-EFM by only requiring a single forward pass to sample the next time step. A well calibrated ensemble should have  $SSR \approx 1$ , yet all models exhibit some degree of underdispersion. CRPS-LAM achieves ensemble calibration comparable to the best-performing model, Graph-EFM, whereas Diffusion-LAM shows stronger underdispersion, particularly at longer lead times. By investigating the spectra of the fields produced by the models in Fig. 4 we also note that CRPS-LAM retains more fine-scale details than Graph-EFM, but lose some of the highest frequency components still captured by Diffusion-LAM. More detailed results are shown in Appendix C.

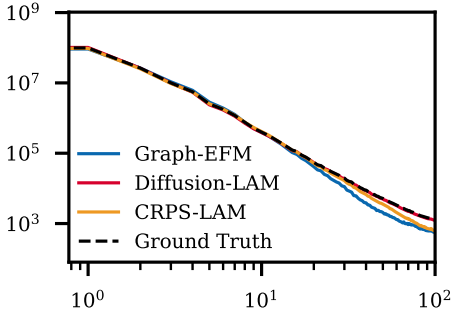


Figure 4: Energy spectra of humidity at 57 h. Diffusion-LAM captures the highest frequency components.

## 4 Conclusion

This work introduces CRPS-LAM, a new efficient probabilistic limited-area weather forecasting model that is competitive with diffusion-based baselines and outperforms existing latent-variable approaches. We demonstrate that CRPS-LAM produces skillful forecasts on the MEPS LAM dataset, while retaining highly efficient sampling. Interesting directions for future research include exploring new ways to incorporate latent variables into the model to enhance performance. Further performance improvements could likely also be gained by increasing the model size or exploring more advanced training strategies, such as extending the number of autoregressive training steps.

## Acknowledgements

This research is financially supported by the Swedish Research Council (grant no: 2020-04122, 2024-05011) the Wallenberg AI, Autonomous Systems and Software Program (WASP) funded by the Knut and Alice Wallenberg Foundation, and the Excellence Center at Linköping–Lund in Information Technology (ELLIIT). Our computations were enabled by the Berzelius resource at the National Supercomputer Centre, provided by the Knut and Alice Wallenberg Foundation. Landelius was funded by the Swedish Energy Agency and the European Union’s Horizon 2020 research and innovation programme under grant agreement no. 883973–EnerDigit.

## References

- Daniel Abdi, Isidora Jankov, Paul Madden, Vanderlei Vargas, Timothy A Smith, Sergey Frolov, Montgomery Flora, and Corey Potvin. HRRRCast: a data-driven emulator for regional weather forecasting at convection allowing scales. *arXiv preprint arXiv:2507.05658*, 2025.
- Ferran Alet, Ilan Price, Andrew El-Kadi, Dominic Masters, Stratis Markou, Tom R. Andersson, Jacklynn Stott, Remi Lam, Matthew Willson, Alvaro Sanchez-Gonzalez, and Peter Battaglia. Skillful joint probabilistic weather forecasting from marginals, 2025. URL <https://arxiv.org/abs/2506.10772>.
- Kaifeng Bi, Lingxi Xie, Hengheng Zhang, Xin Chen, Xiaotao Gu, and Qi Tian. Accurate medium-range global weather forecasting with 3d neural networks. *Nature*, 619(7970):533–538, 2023.
- Boris Bonev, Thorsten Kurth, Ankur Mahesh, Mauro Bisson, Jean Kossaifi, Karthik Kashinath, Anima Anandkumar, William D. Collins, Michael S. Pritchard, and Alexander Keller. FourCastNet 3: A geometric approach to probabilistic machine-learning weather forecasting at scale, 2025. URL <http://arxiv.org/abs/2507.12144>.
- Mingjian Chen, Xu Tan, Bohan Li, Yanqing Liu, Tao Qin, Sheng Zhao, and Tie-Yan Liu. Adaspeech: Adaptive text to speech for custom voice, 2021. URL <https://arxiv.org/abs/2103.00993>.
- C. A. T. Ferro. Fair scores for ensemble forecasts. *Quarterly Journal of the Royal Meteorological Society*, 140(683):1917–1923, 2014. doi: <https://doi.org/10.1002/qj.2270>. URL <https://rmets.onlinelibrary.wiley.com/doi/abs/10.1002/qj.2270>.
- Tilmann Gneiting and Adrian E. Raftery. Strictly proper scoring rules, prediction, and estimation. *Journal of the American Statistical Association*, pages 359–378, 2007.
- Tero Karras, Miika Aittala, Timo Aila, and Samuli Laine. Elucidating the design space of diffusion-based generative models. In *Proc. NeurIPS*, 2022.
- Remi Lam, Alvaro Sanchez-Gonzalez, Matthew Willson, Peter Wirnsberger, Meire Fortunato, Ferran Alet, Suman Ravuri, Timo Ewalds, Zach Eaton-Rosen, Weihua Hu, et al. Learning skillful medium-range global weather forecasting. *Science*, 382(6677):1416–1421, 2023.
- Simon Lang, Mihai Alexe, Matthew Chantry, Jesper Dramsch, Florian Pinault, Baudouin Raoult, Mariana C. A. Clare, Christian Lessig, Michael Maier-Gerber, Linus Magnusson, Zied Ben Bouallègue, Ana Prieto Nemesio, Peter D. Dueben, Andrew Brown, Florian Pappenberger, and Florence Rabier. AIFS – ECMWF’s data-driven forecasting system, 2024a. URL <https://arxiv.org/abs/2406.01465>.
- Simon Lang, Mihai Alexe, Mariana C. A. Clare, Christopher Roberts, Rilwan Adewoyin, Zied Ben Bouallègue, Matthew Chantry, Jesper Dramsch, Peter D. Dueben, Sara Hahner, Pedro Maciel, Ana Prieto-Nemesio, Cathal O’Brien, Florian Pinault, Jan Polster, Baudouin Raoult, Steffen Tietsche, and Martin Leutbecher. AIFS-CRPS: Ensemble forecasting using a model trained with a loss function based on the continuous ranked probability score, 2024b. URL <https://arxiv.org/abs/2412.15832>.
- Simon Lang, Martin Leutbecher, and Pedro Maciel. A multi-scale loss formulation for learning a probabilistic model with proper score optimisation, 2025. URL <http://arxiv.org/abs/2506.10868>.

- Erik Larsson, Joel Oskarsson, Tomas Landelius, and Fredrik Lindsten. Diffusion-lam: Probabilistic limited area weather forecasting with diffusion. In *ICLR 2025 Workshop on Tackling Climate Change with Machine Learning*, 2025. URL <https://www.climatechange.ai/papers/iclr2025/36>.
- Joel Oskarsson, Tomas Landelius, and Fredrik Lindsten. Graph-based neural weather prediction for limited area modeling. In *NeurIPS 2023 Workshop on Tackling Climate Change with Machine Learning*, 2023.
- Joel Oskarsson, Tomas Landelius, Marc Peter Deisenroth, and Fredrik Lindsten. Probabilistic weather forecasting with hierarchical graph neural networks. In *Advances in Neural Information Processing Systems*, volume 37, 2024.
- Lorenzo Pacchiardi, Rilwan A. Adewoyin, Peter Dueben, and Ritabrata Dutta. Probabilistic forecasting with generative networks via scoring rule minimization. 25(45):1–64, 2024. ISSN 1533-7928. URL <http://jmlr.org/papers/v25/23-0038.html>.
- Jaideep Pathak, Yair Cohen, Piyush Garg, Peter Harrington, Noah Brenowitz, Dale Durran, Morteza Mardani, Arash Vahdat, Shaoming Xu, Karthik Kashinath, and Michael Pritchard. Kilometer-scale convection allowing model emulation using generative diffusion modeling, 2024. URL <https://arxiv.org/abs/2408.10958>.
- Ilan Price, Alvaro Sanchez-Gonzalez, Ferran Alet, Tom R Andersson, Andrew El-Kadi, Dominic Masters, Timo Ewalds, Jacklynn Stott, Shakir Mohamed, Peter Battaglia, et al. Probabilistic weather forecasting with machine learning. *Nature*, 637(8044):84–90, 2025.
- Yang Song, Jascha Sohl-Dickstein, Diederik P Kingma, Abhishek Kumar, Stefano Ermon, and Ben Poole. Score-based generative modeling through stochastic differential equations. In *International Conference on Learning Representations*, 2021.

## A Table of notation

The notation that is used in this paper is summarized in Table 1.

Table 1: Table of notation.

Notation	Description
$X^t$	Full weather state including both the interior and the boundary at lead time $t$
$X_I^t$	Interior of weather state at lead time $t$
$X_B^t$	Boundary of weather state at lead time $t$
$X_{g,d}^t$	Weather variable $d$ at grid position $g$ at lead time $t$
$\hat{X}_{g,d}^t$	Predicted weather variable $d$ at grid position $g$ at lead time $t$
$G$	The grid points in a full weather state $X^t$
$G_I$	The grid points in the interior of a weather state $X_I^t$
$F^t$	Forcing variables at lead time $t$
$S$	Static variables for each position in the grid $G$
$I^t$	Interior input $\{X_I^{t-1:t}, F_I^{t-1:t+1}, S_I\}$ at lead time $t$
$B^t$	Boundary input $\{X_B^{t-1:t+1}, F_B^{t-1:t+1}, S_B\}$ at lead time $t$
$d_x$	The number of weather variables in each grid cell of each state $X^t$
$T$	Number of forecast steps in a sampled trajectory
$N$	Number of ensemble members
$z$	Latent noise vector

## B Experiment Details

An overview schematic of our architecture of our backbone model is shown in Fig. 5 with the details of each U-Net shown in Fig. 6. Note that the MLP blocks are different from the U-Net blocks and consist of a two-layer MLP followed by a conditional layer normalization, where the latent variable  $z$  is included as an additional conditioning input.

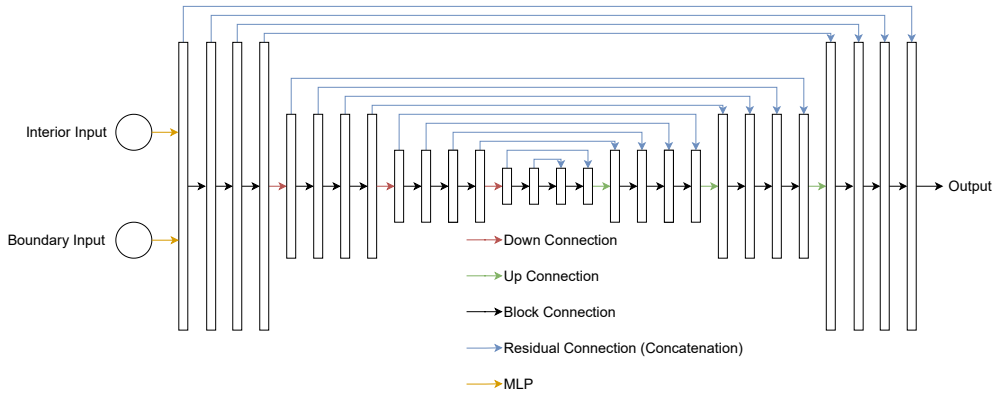


Figure 5: An overview of the backbone model.

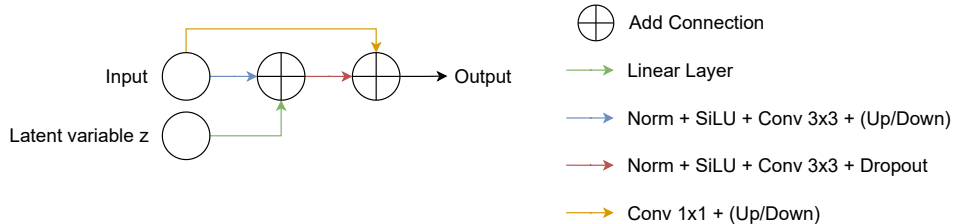


Figure 6: A description of each U-Net block.

The training procedure for CRPS-LAM is summarized in Table 2. We begin by training the model on single-step forecasts until convergence, after which we extend the training to two-step autoregressive rollouts. In this setup, we did not observe any additional benefits from training with more autoregressive steps.

Table 2: Training schedule.

Epochs	Learning Rate	Autoregressive Steps
600	0.001	1
400	0.0001	1
200	0.00001	2

During the initial training phase, we sometimes observe instability where the model collapses into producing near-deterministic forecasts, effectively minimizing the mean absolute error of each ensemble member while neglecting the latent variable. Similar behavior has been reported by Lang et al. [2024b], who proposed a modified training objective to address it, and by Bonev et al. [2025], who mitigated the issue by using a biased CRPS estimator with a large ensemble early in training, later transitioning to a smaller ensemble and the unbiased fair CRPS estimator.

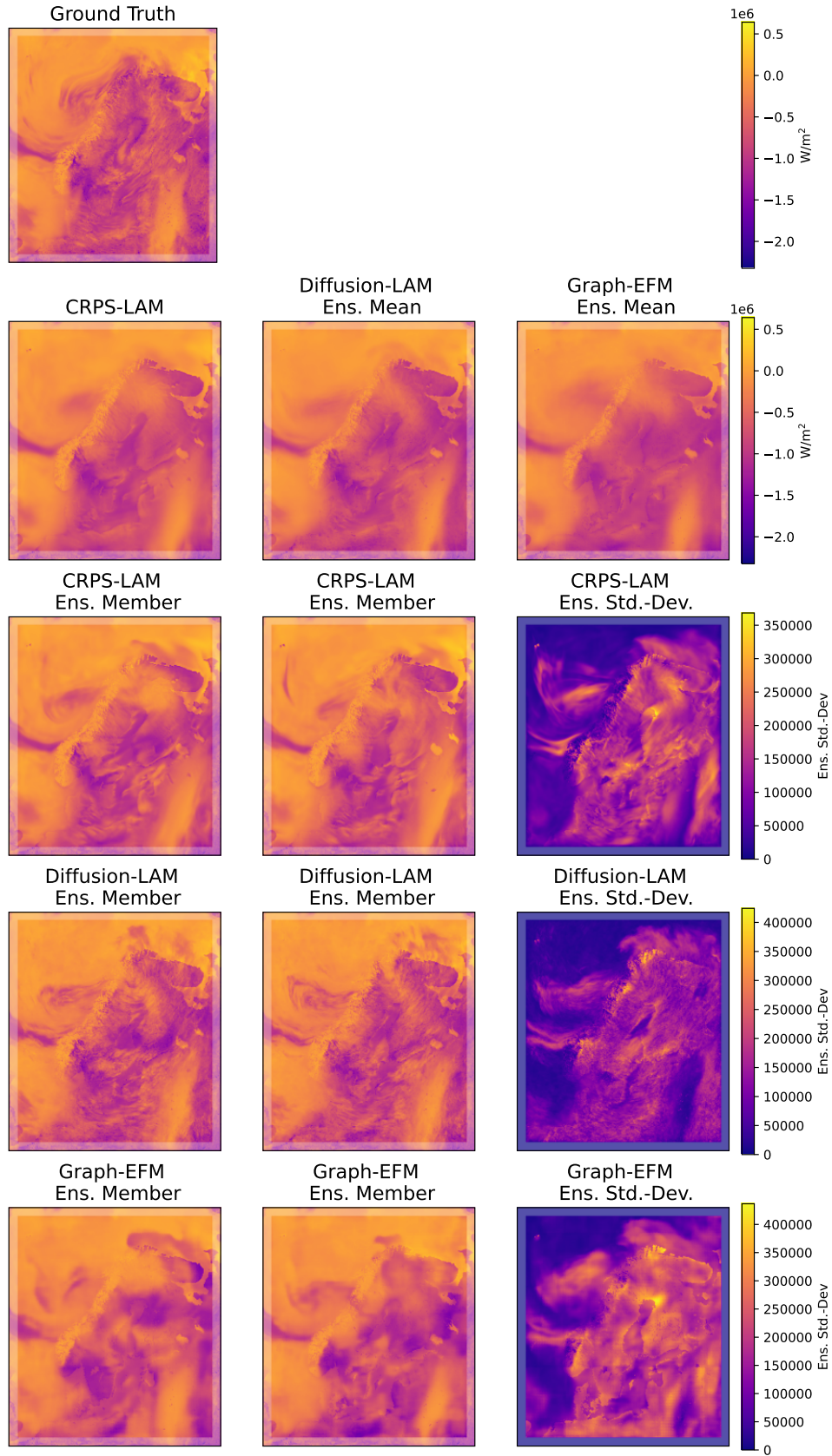
Prior to introducing autoregressive training with two-step trajectories, we observed artifacts in a small subset of ensemble members at longer lead times. However, these artifacts disappeared once the model was trained with autoregressive forecasting steps, suggesting that training with multiple autoregressive steps helps stabilize the usage of latent variables at longer lead times.

In contrast to Graph-EFM and Diffusion-LAM, we do not apply any weighting of the loss function across atmospheric levels or variables, as we found it unnecessary to achieve competitive results. However, if it is desired to emphasize specific atmospheric levels or variables, such weighting could easily be incorporated into the loss function within this framework.

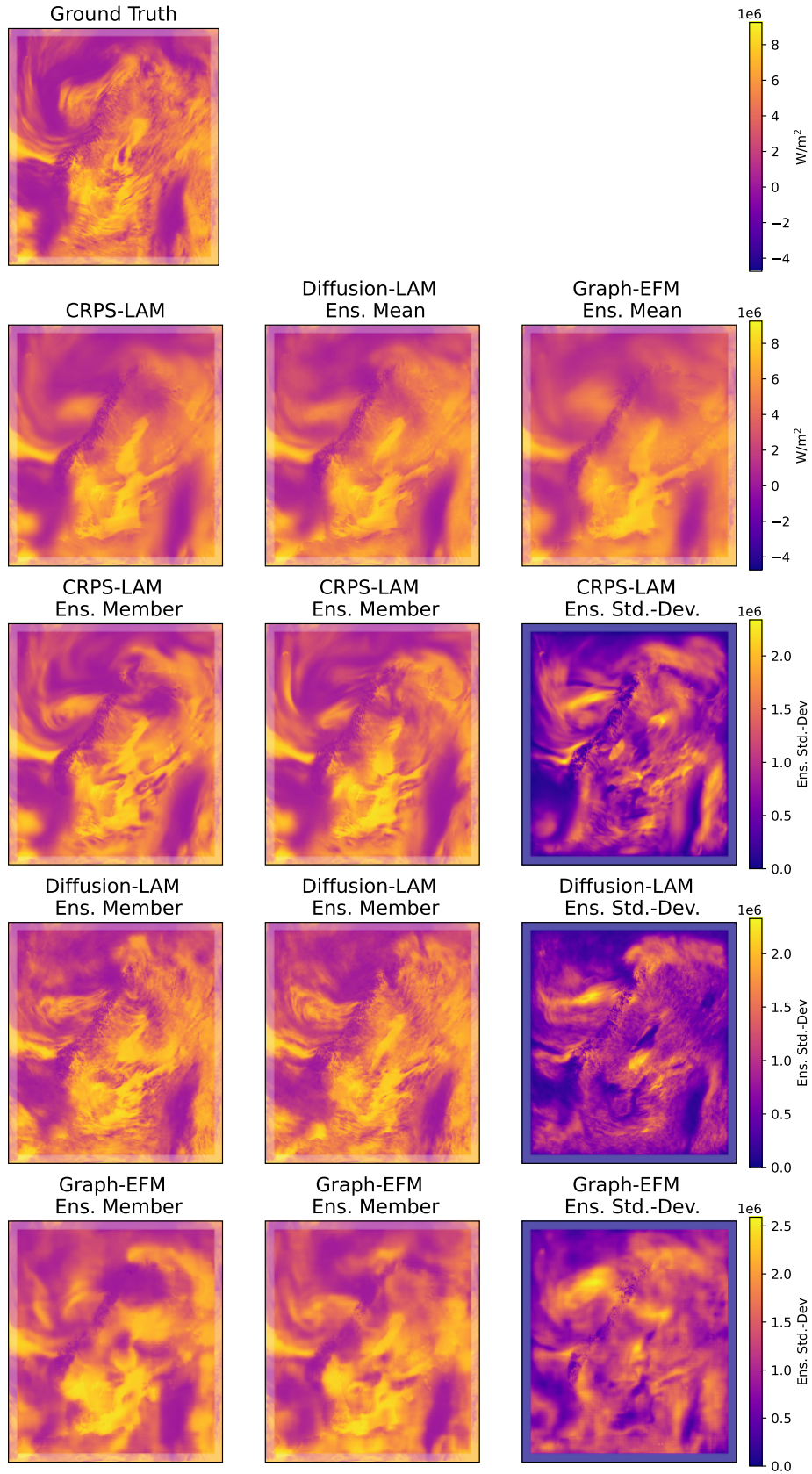
When preparing the dataset, we subsampled every fourth grid point, reducing the spatial resolution from the native 2.5 km of MEPS to 10 km. Consequently, spectral components at wavenumbers above  $10^2$  are not physically meaningful, since the models cannot represent scales finer than those resolved by the input data. In an operational setting, such unresolved scales should be suppressed by applying a suitable low-pass filter.

## C Additional results

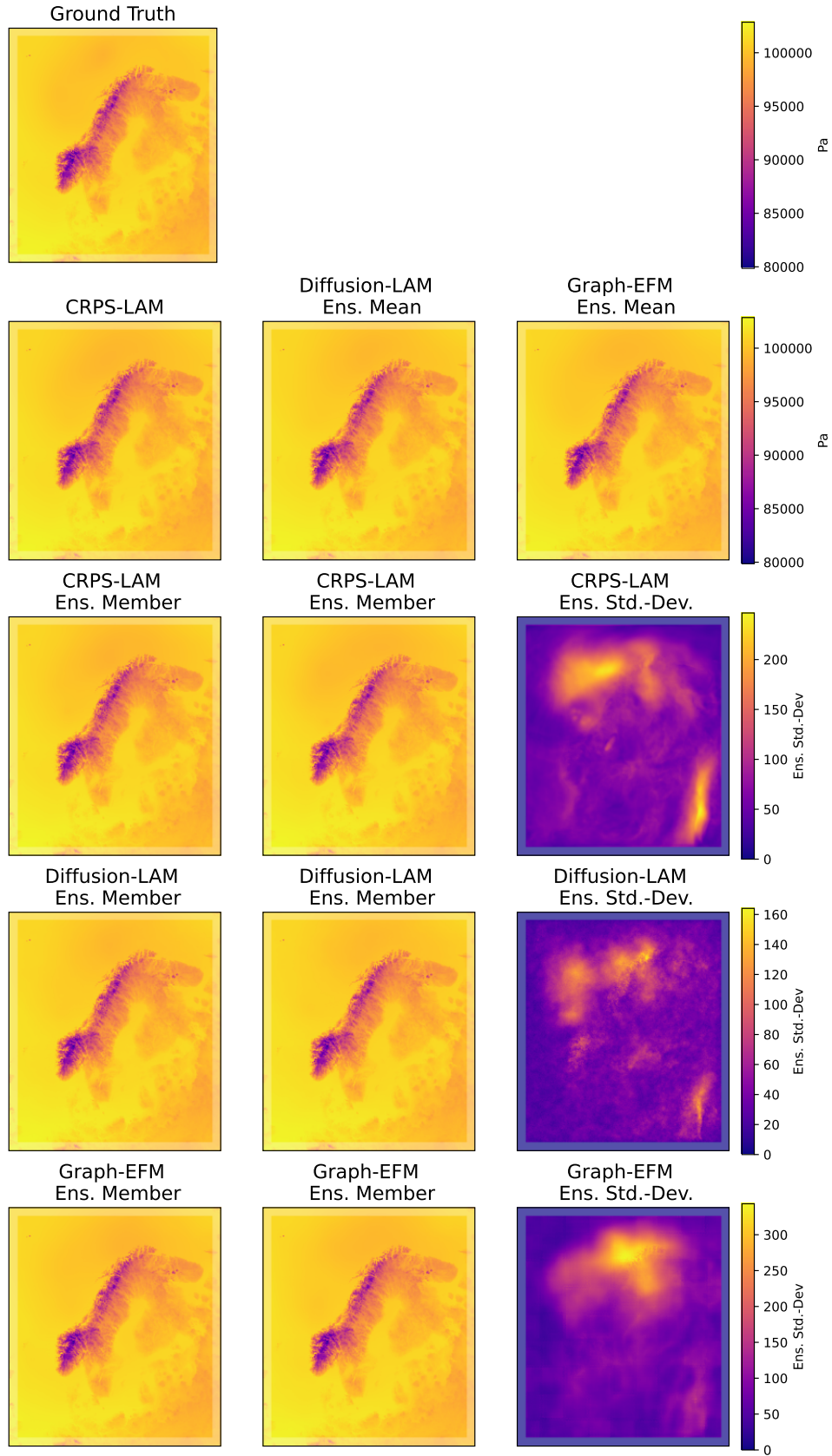
We provide detailed per-variable evaluation results in Fig. 8, Fig. 9, and Fig. 10, together with a 57 h forecast example for a randomly selected test case in Fig. 7. The corresponding energy spectra for all variables are shown in Figs. 11 to 14. For an evaluation of deterministic models and less competitive probabilistic baselines on the MEPS dataset, we refer the reader to Oskarsson et al. [2023, 2024].



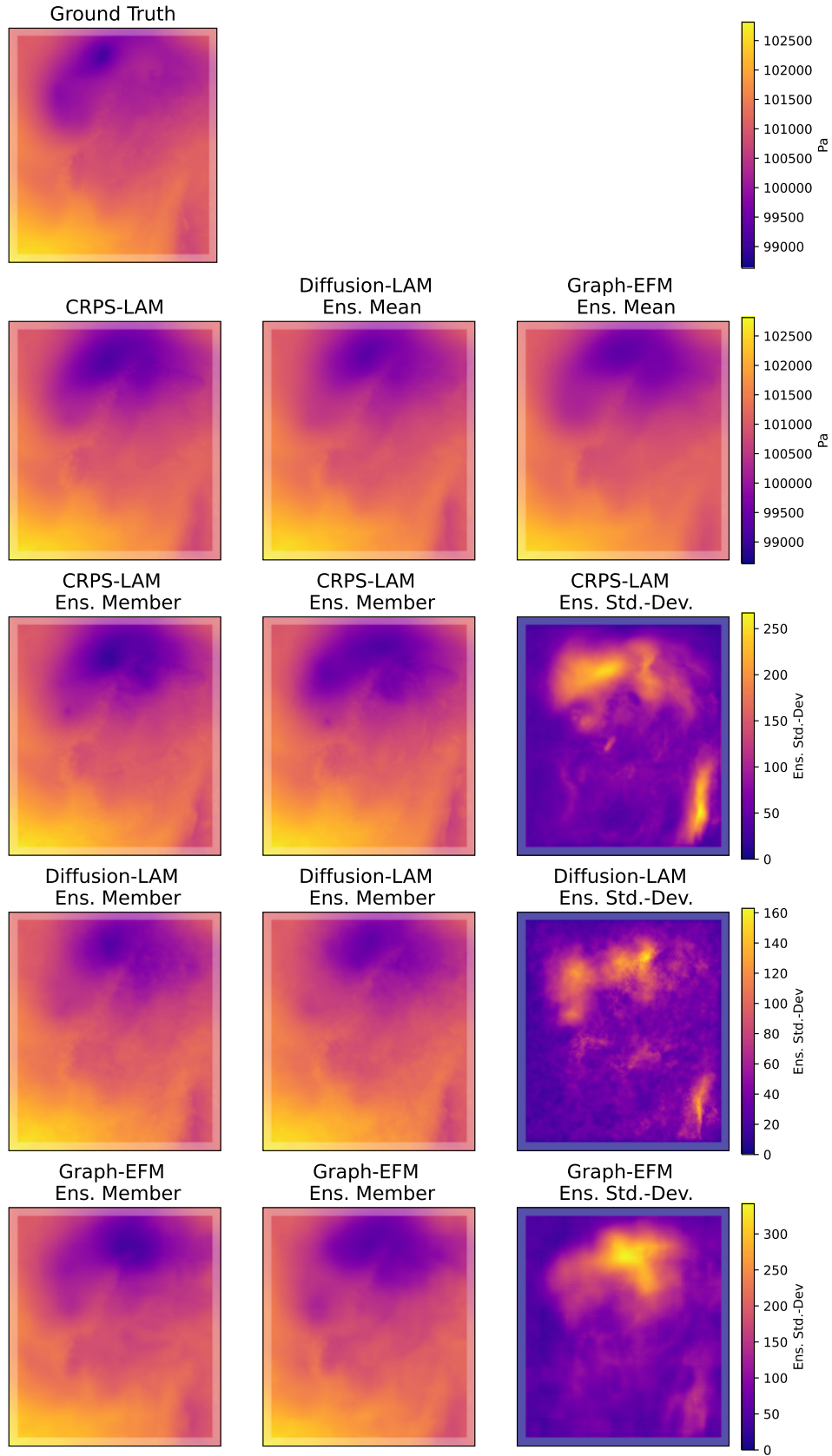
(a) nlwrs\_0



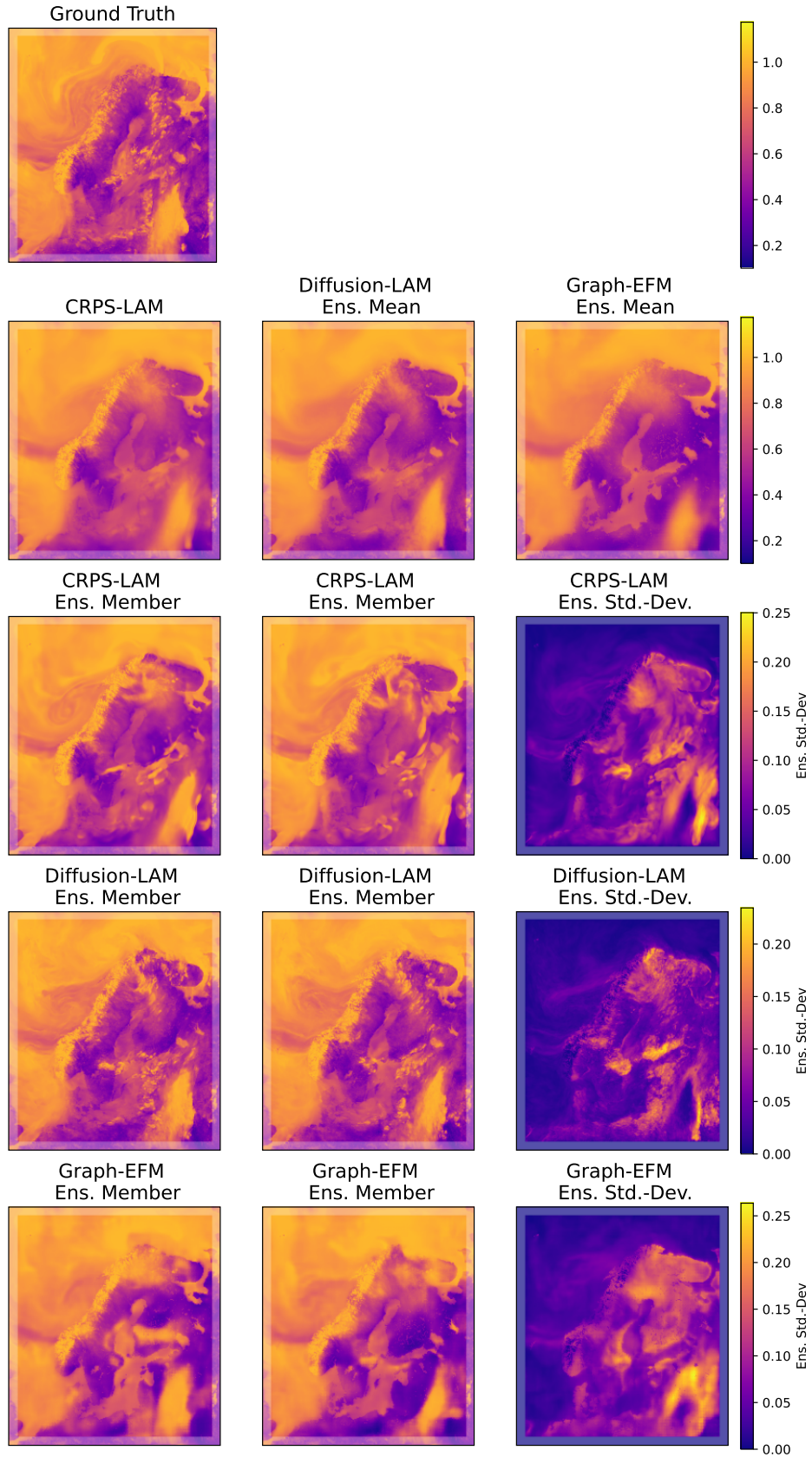
(b) nswrs\_0



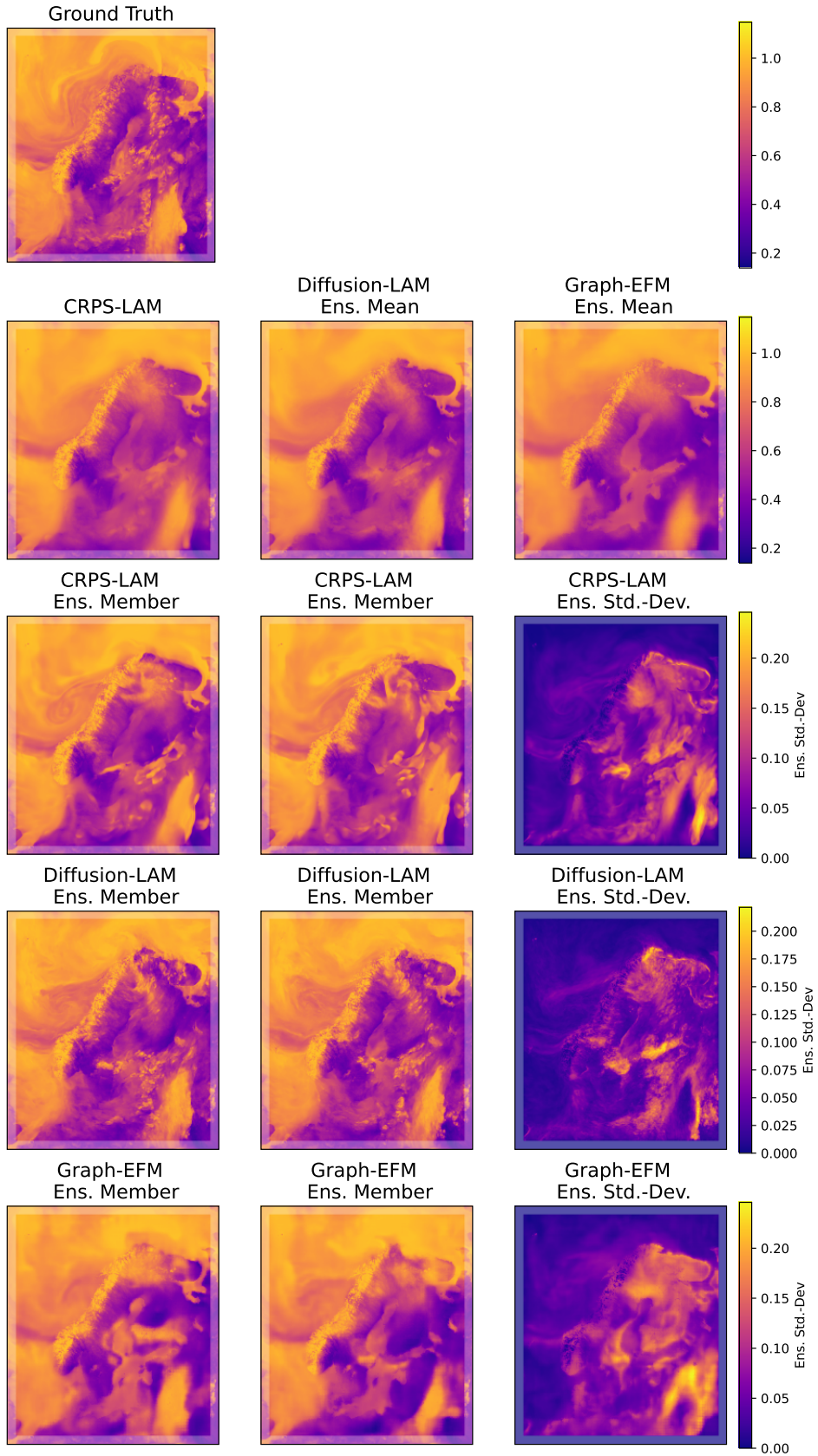
(c) pres\_0g



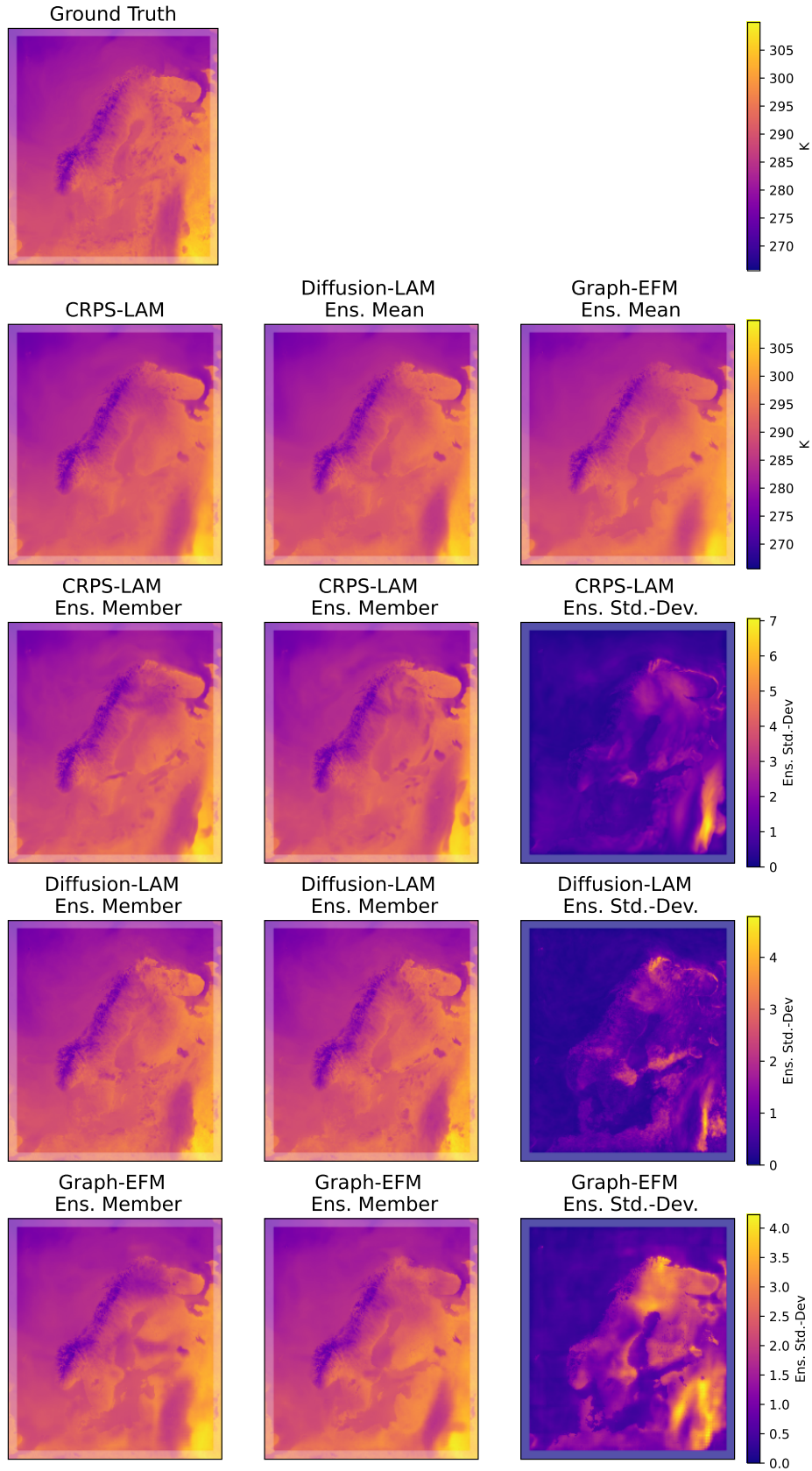
(d) pres\_0s



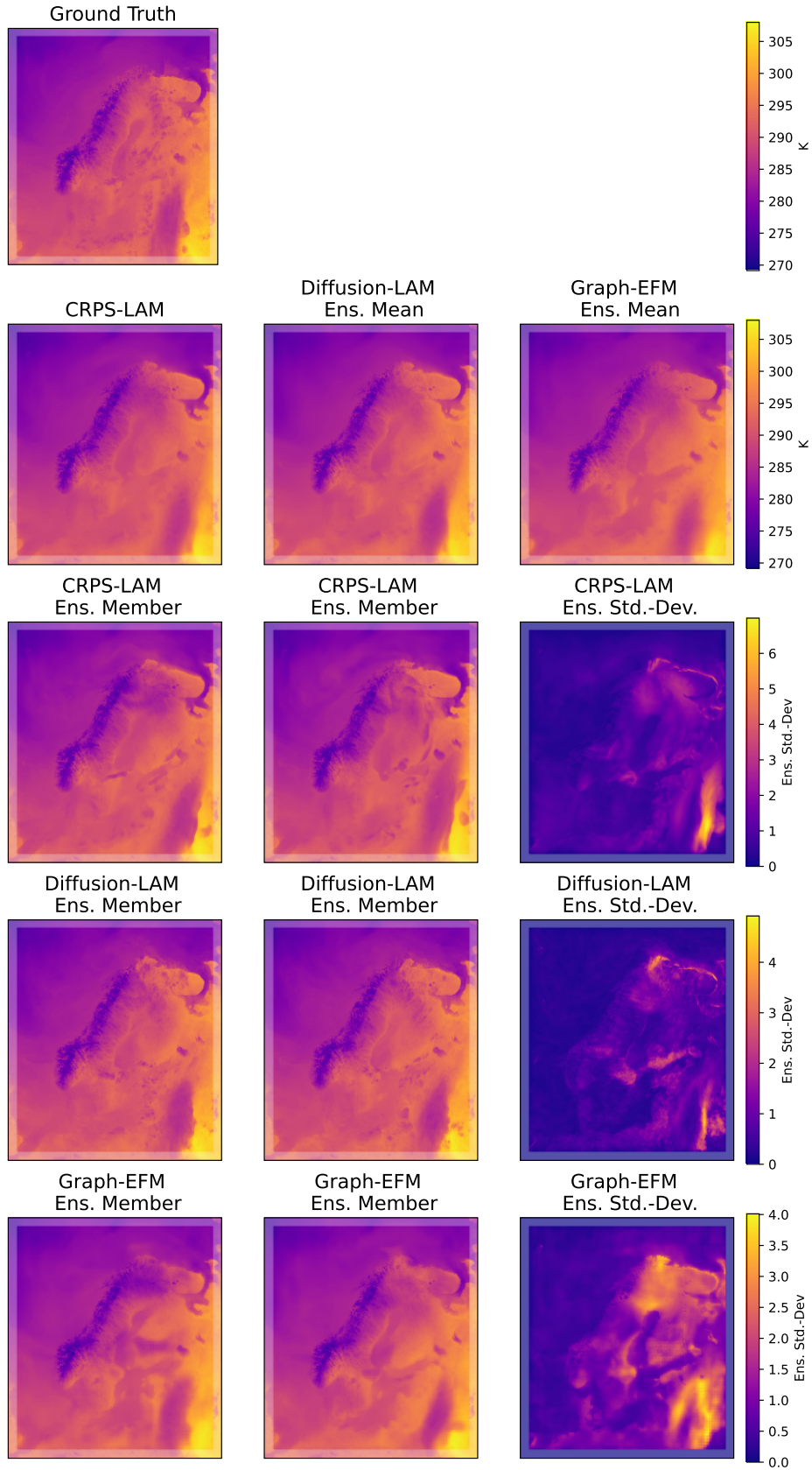
(e) r\_2



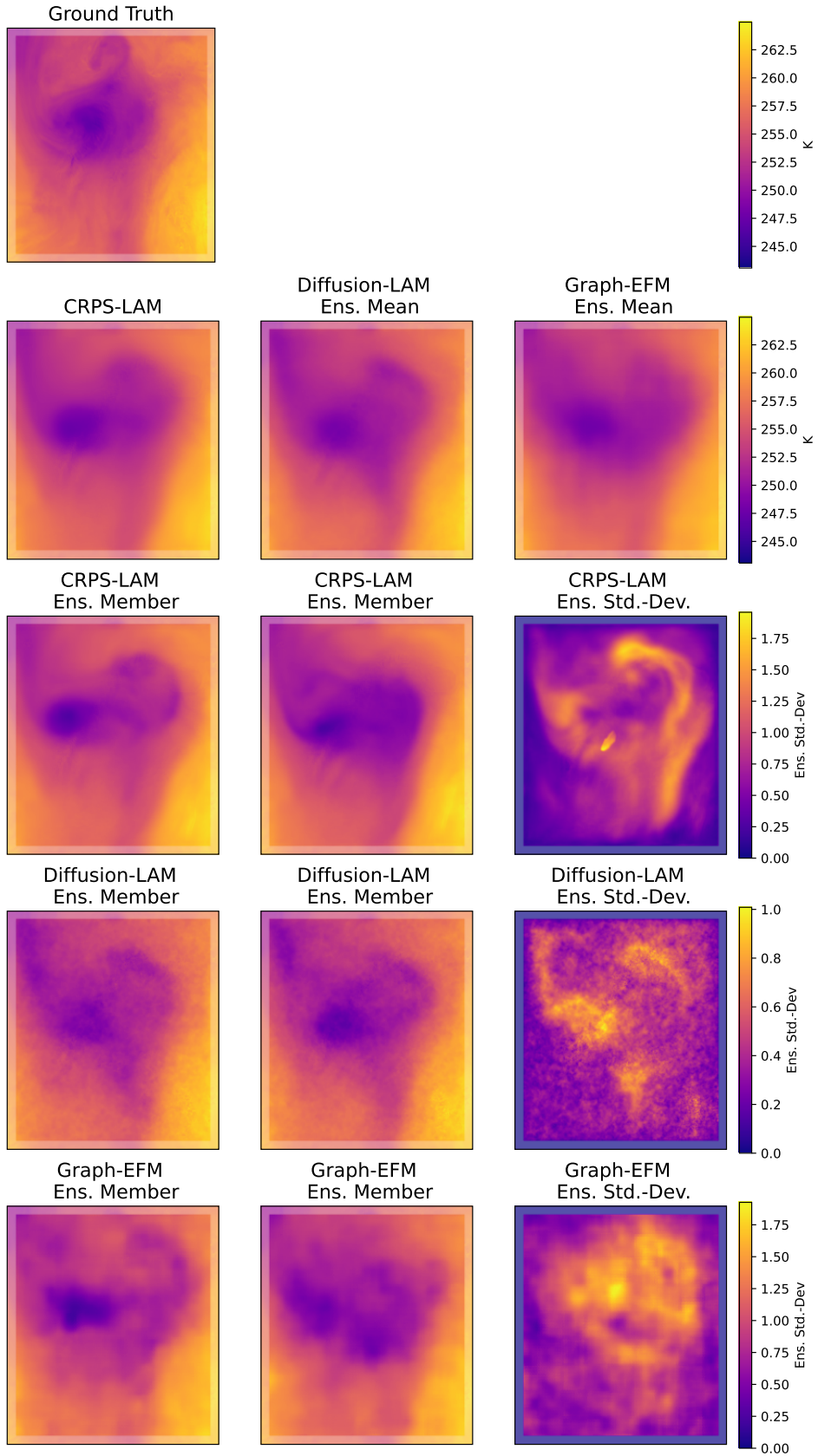
(f) r\_65



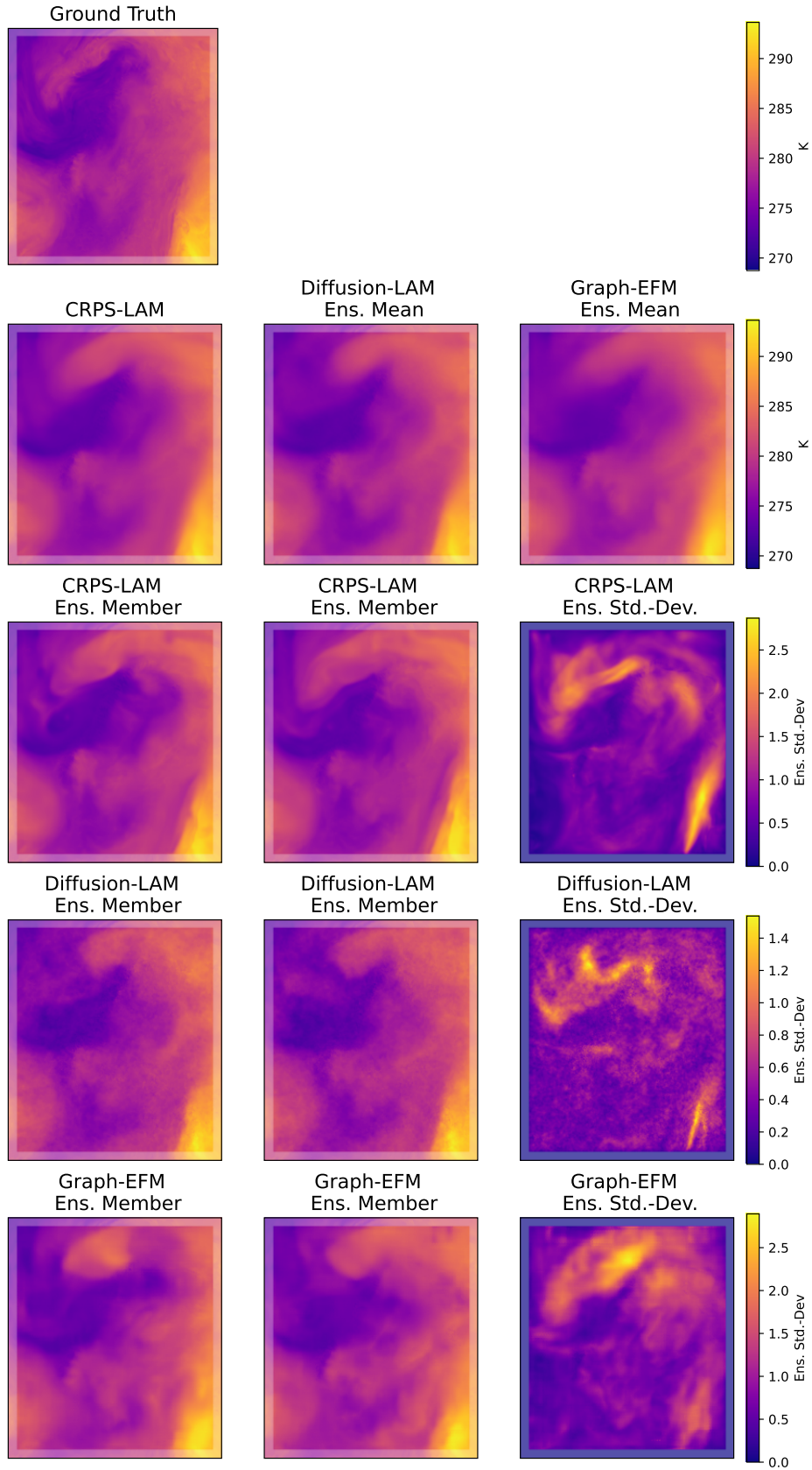
(g)  $\tau_2$



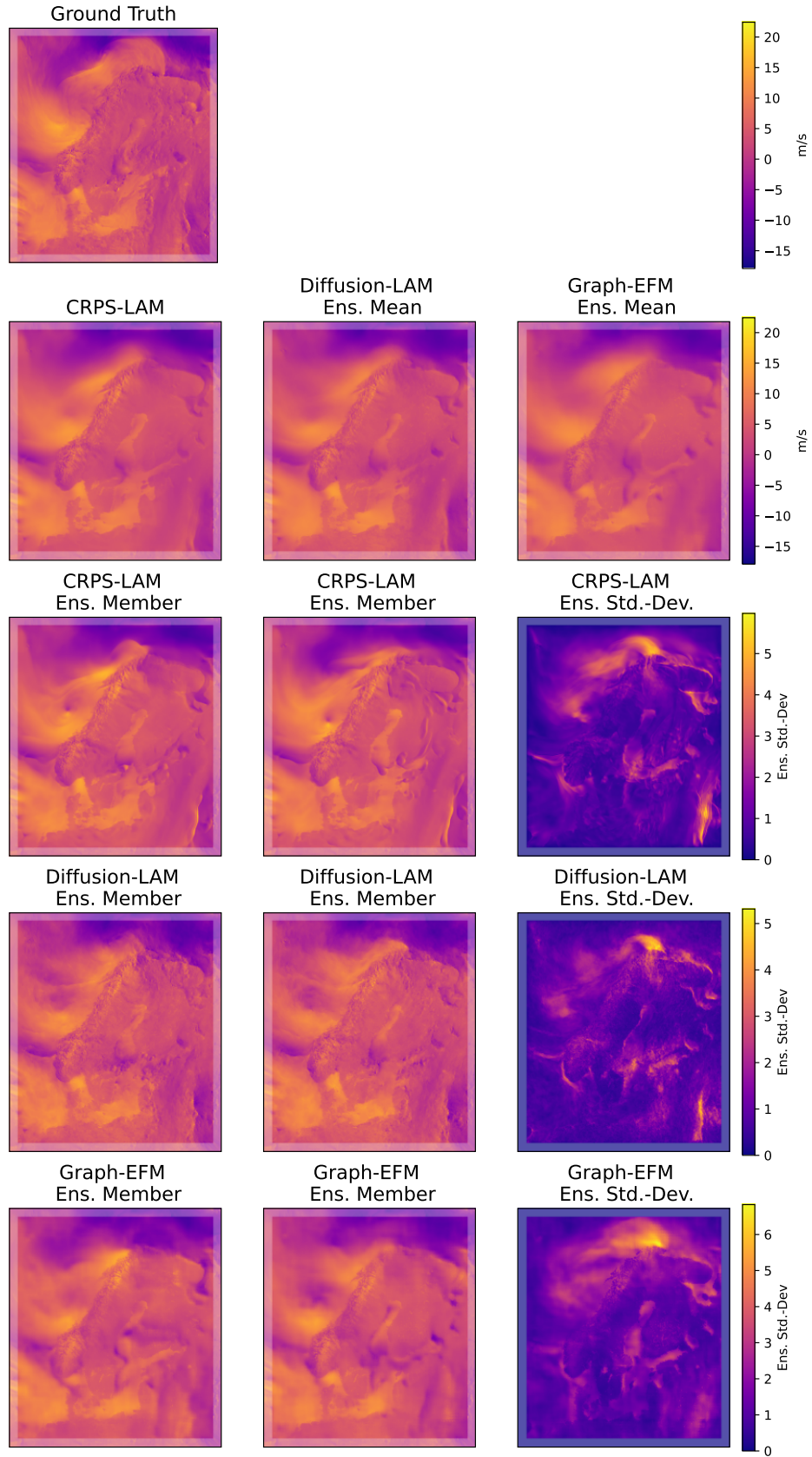
(h)  $t_{500}$



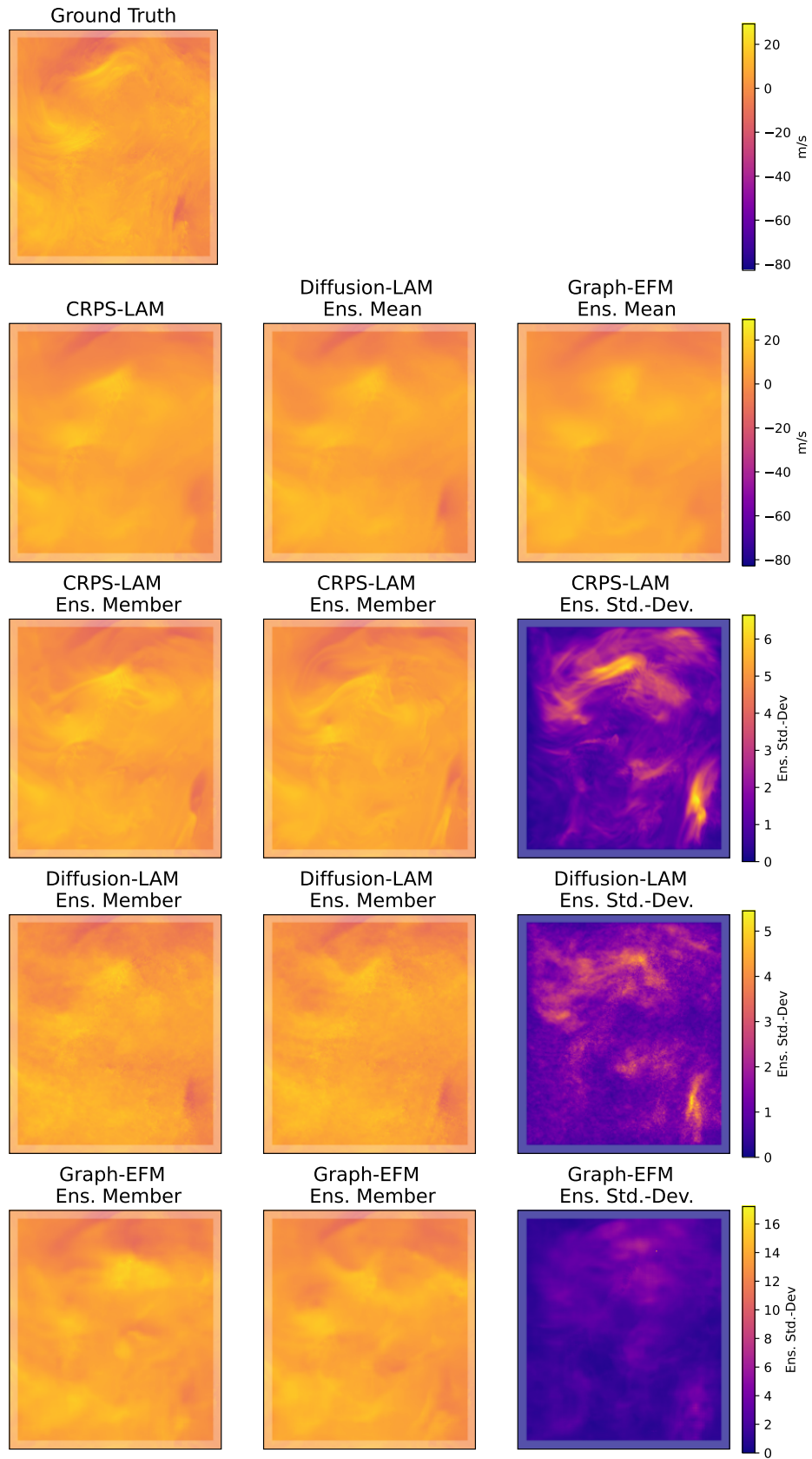
(i)  $t_{65}$



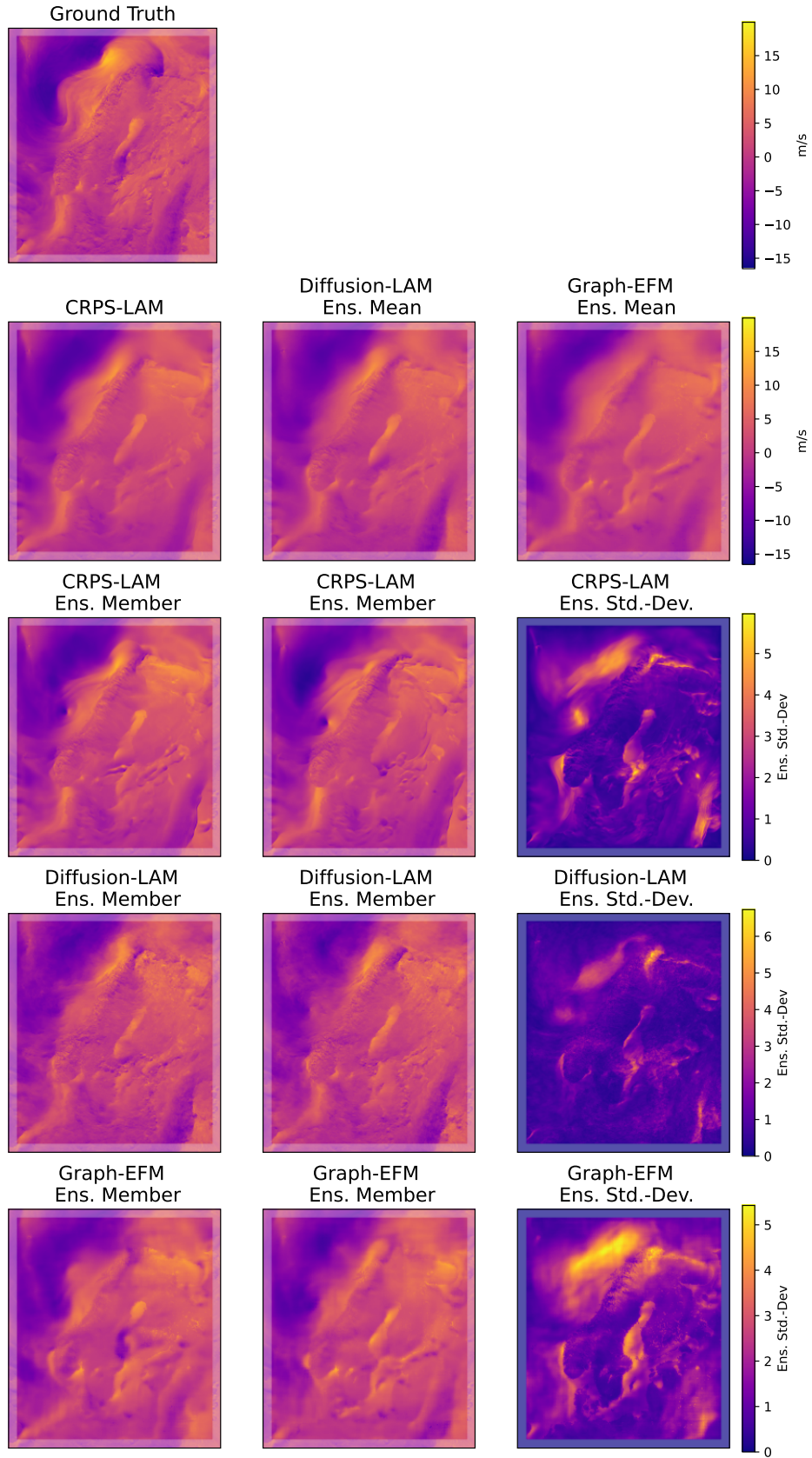
(j)  $\tau_{850}$



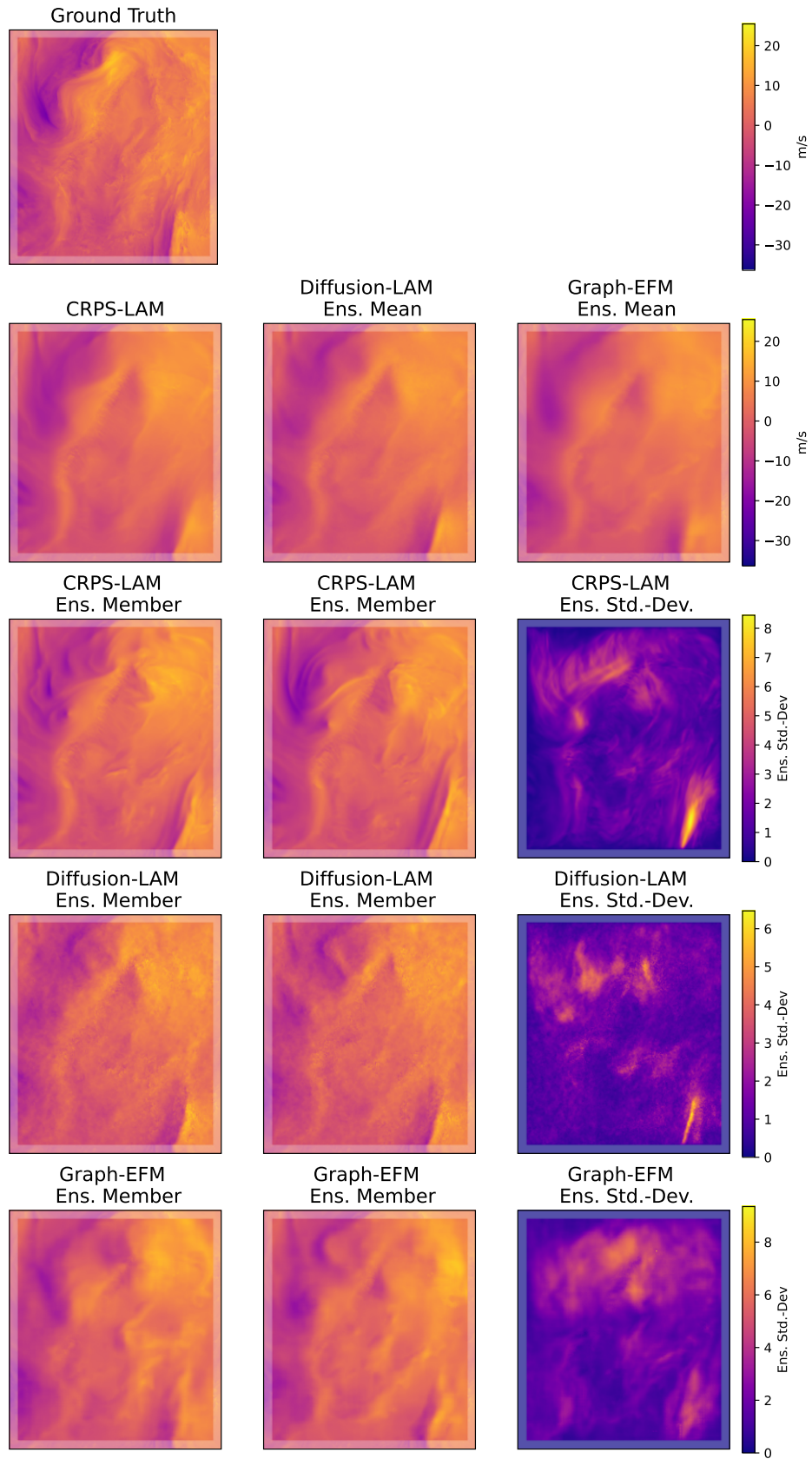
(k)  $u_{65}$



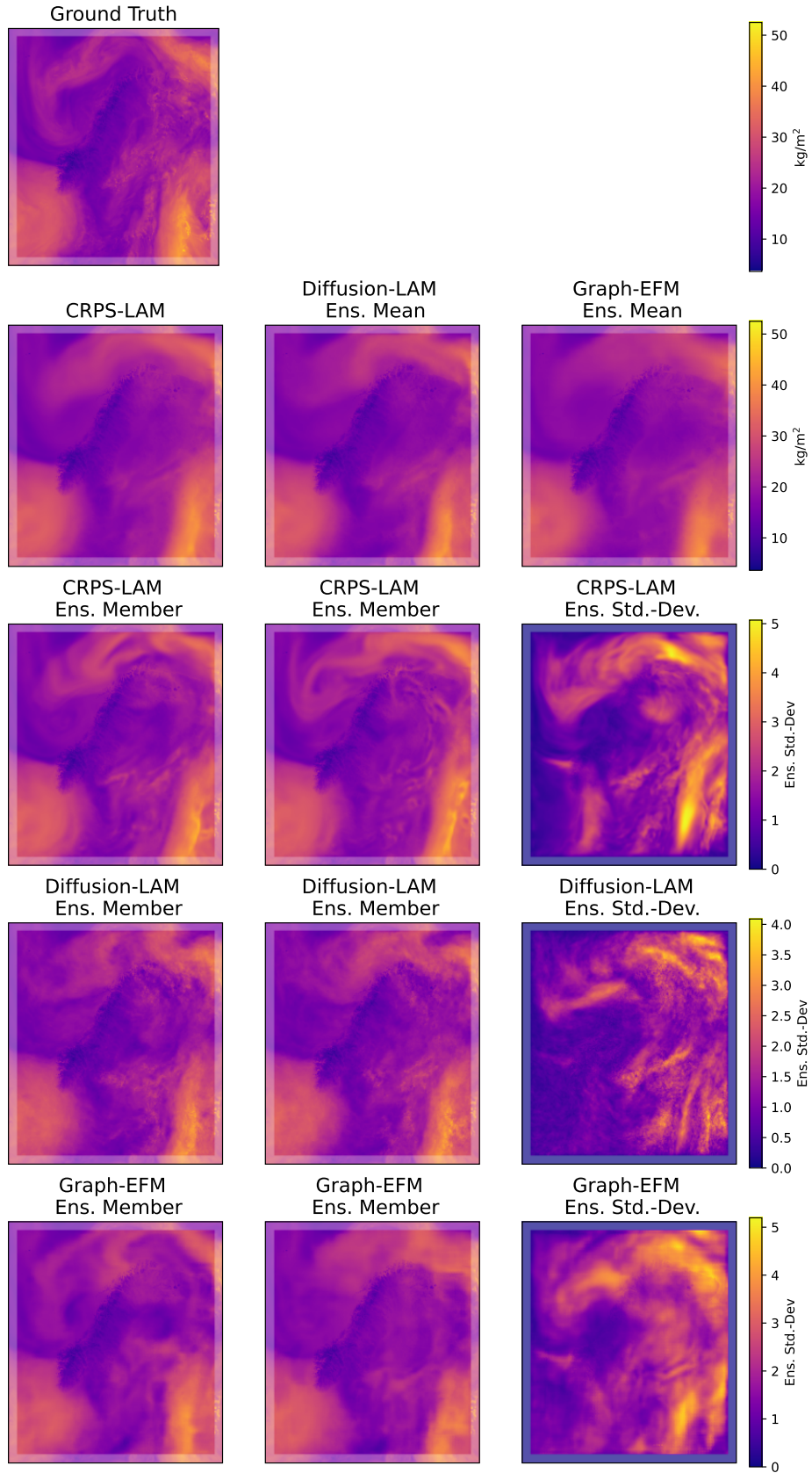
(l)  $u_{850}$



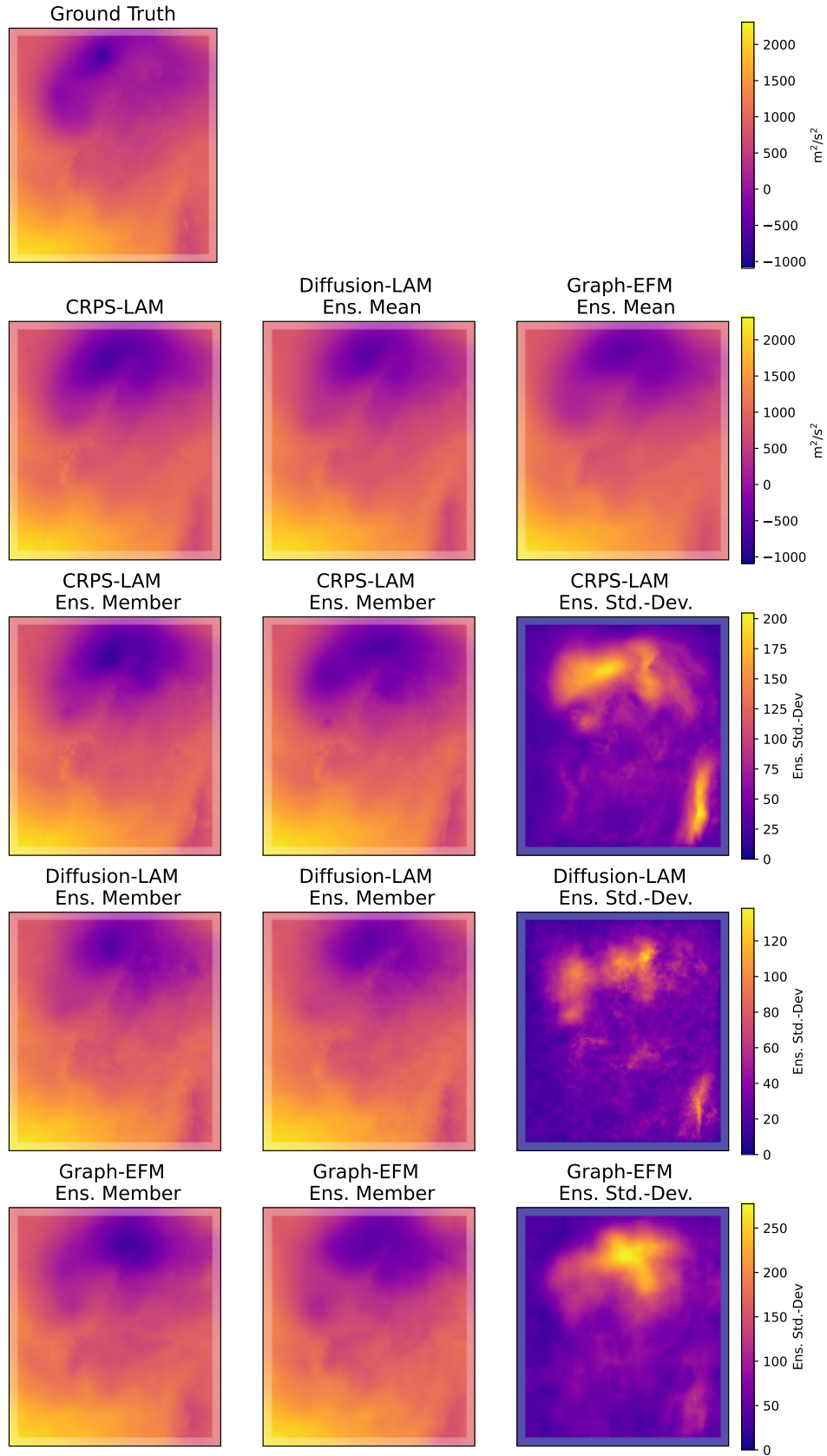
(m) v\_65



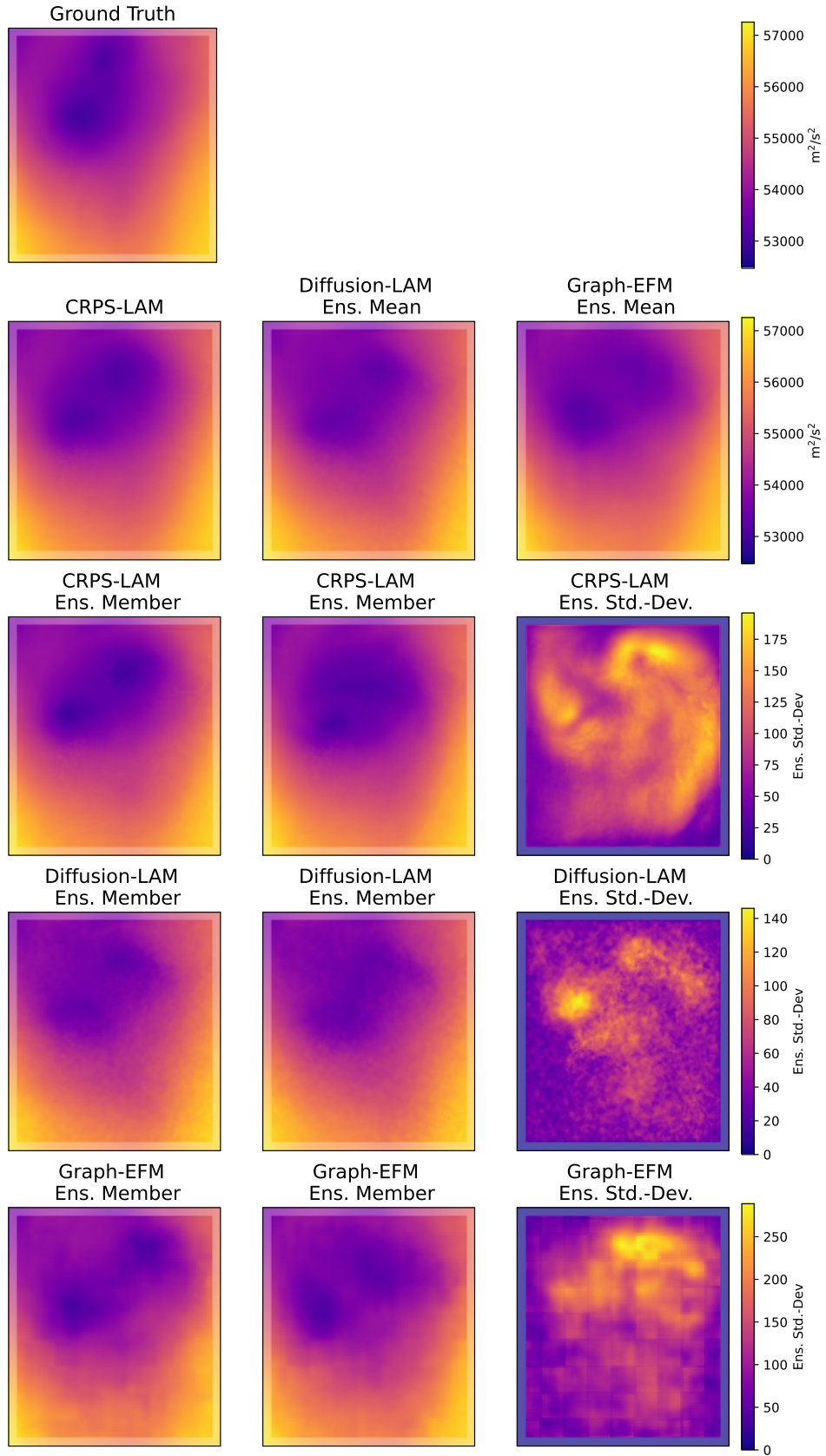
(n) v\_850



(o) wvint\_0



(p)  $z_{1000}$



(q) z\_500

Figure 7: An ensemble forecasts for each variable at 57 h.

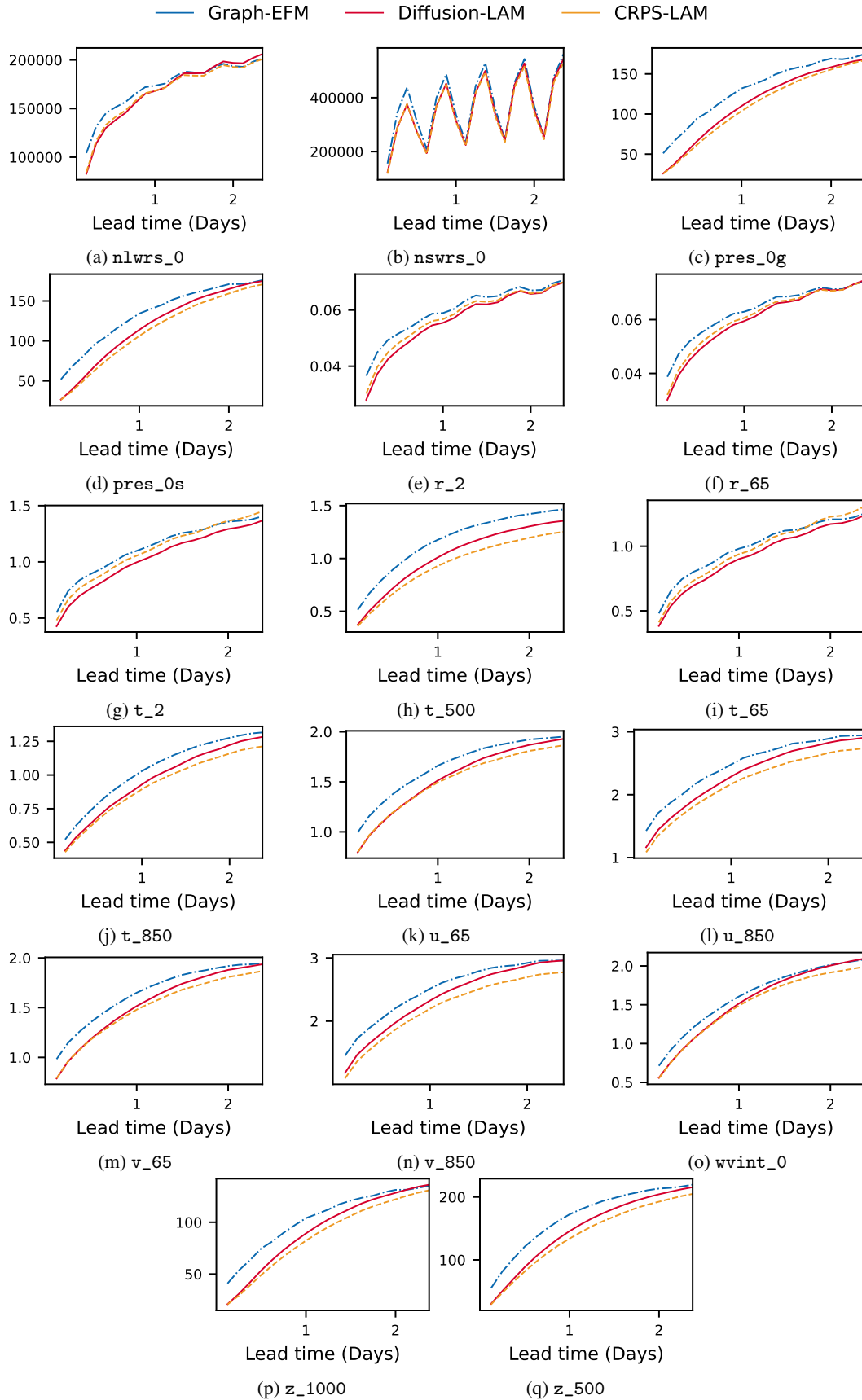


Figure 8: The RMSE results for each variable.

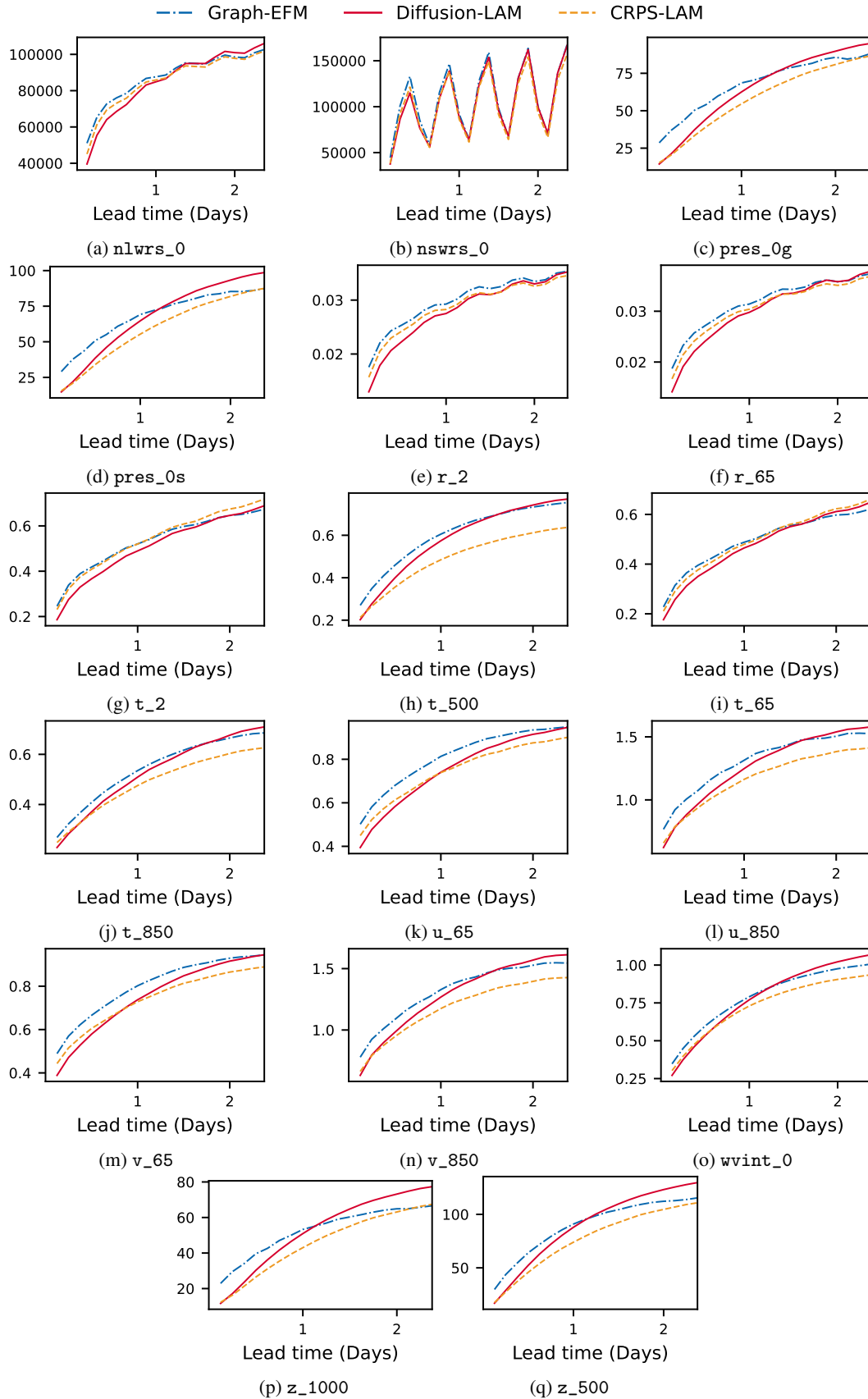


Figure 9: The CRPS results for each variable.

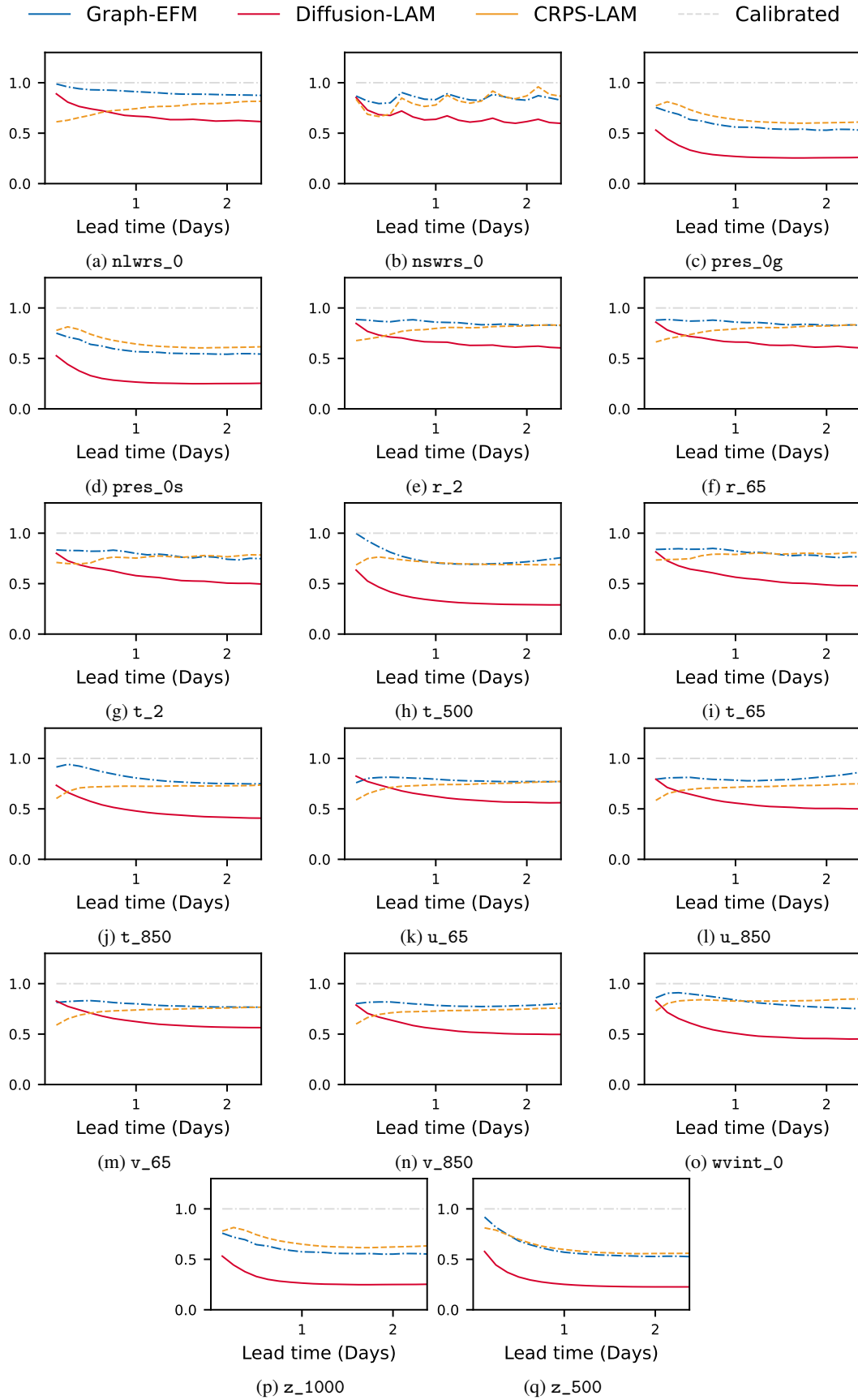


Figure 10: The SSR results for each variable.

— Graph-EFM    — Diffusion-LAM    — CRPS-LAM    - - - - Ground Truth

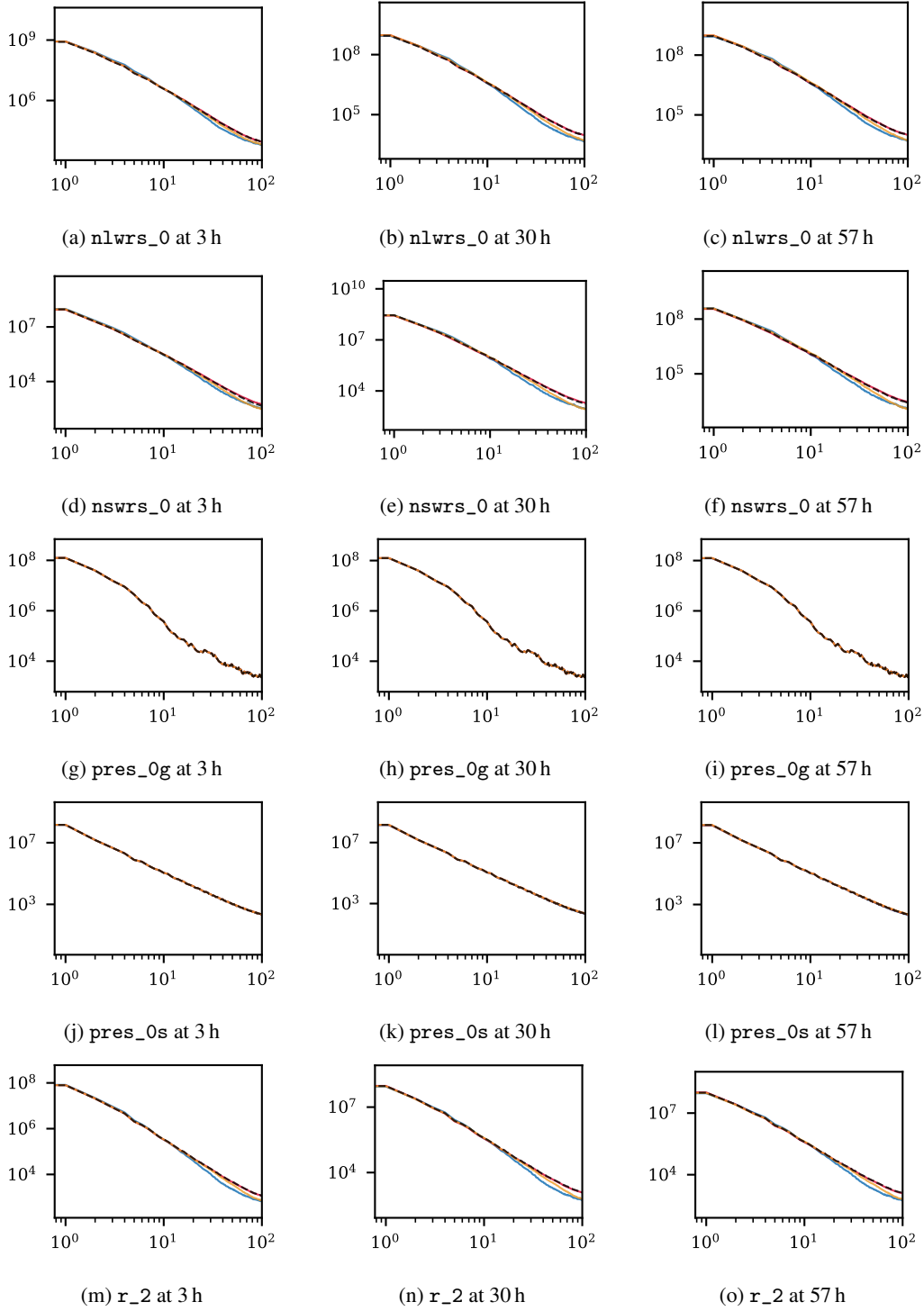


Figure 11: The energy spectra for each variable at the lead times 3 h, 30 h, and 57 h.

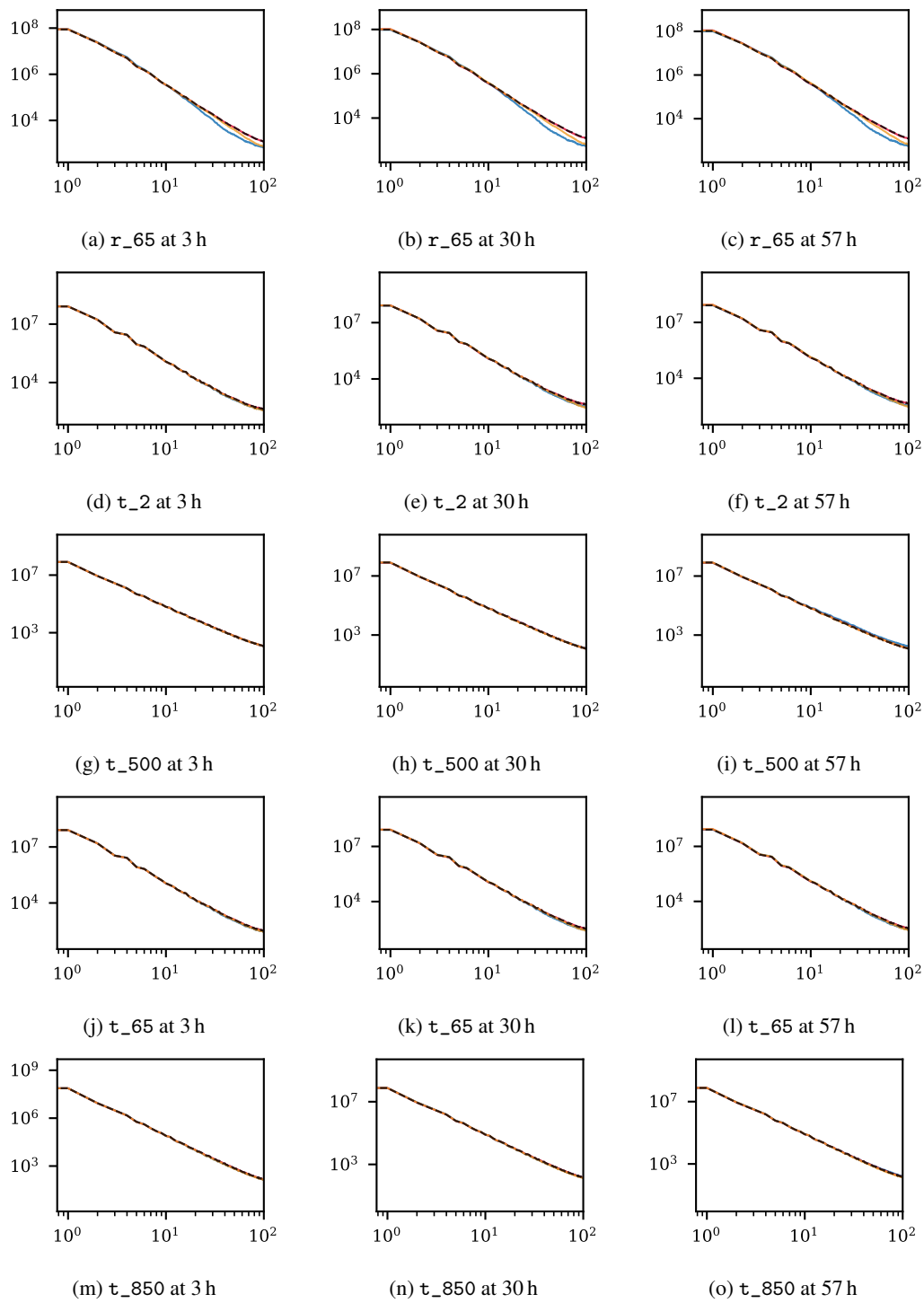


Figure 12: The energy spectra for each variable at the lead times 3 h, 30 h, and 57 h.

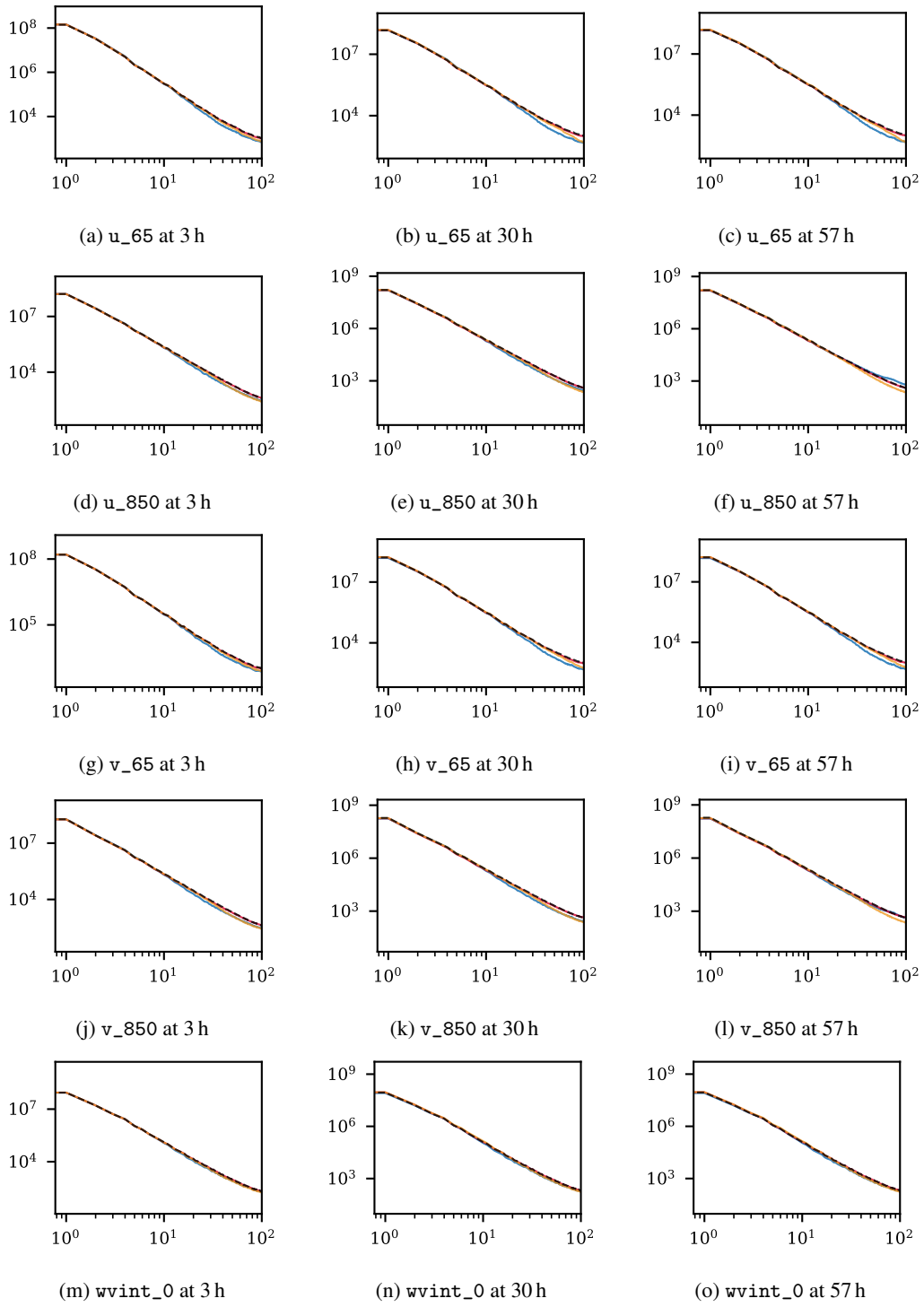


Figure 13: The energy spectra for each variable at the lead times 3 h, 30 h, and 57 h.

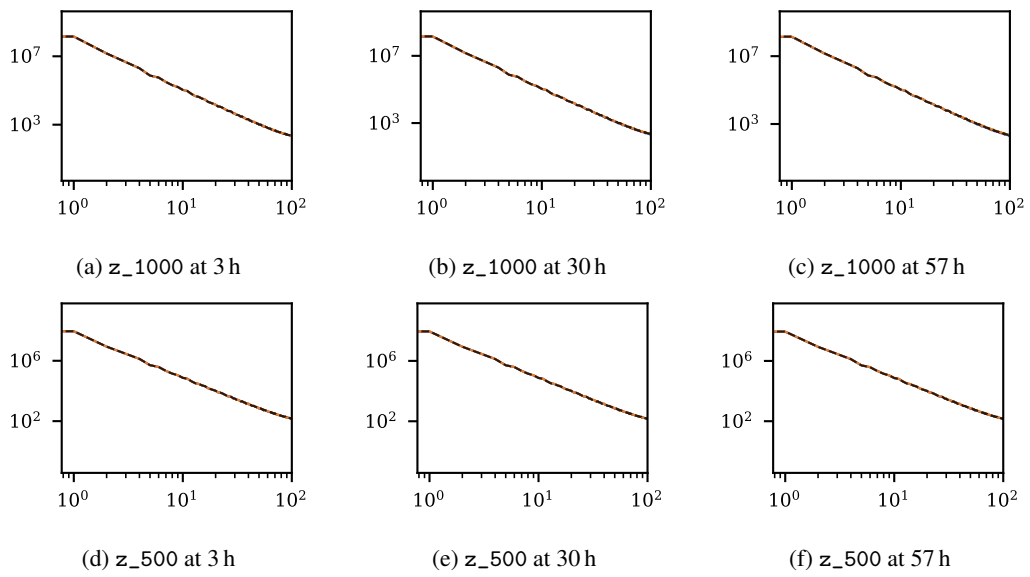


Figure 14: The energy spectra for each variable at the lead times 3 h, 30 h, and 57 h.